Experimental Investigation of Energy Harvesting Eel in the Wake of Bluff Body under Ocean Waves

Author

Ehtisham Ali

Registration Number

171615

Supervisor

Dr. Emad Uddin

DEPARTMENT OF DESIGN & MANUFACTURING ENGINEERING

SCHOOL OF MECHANICAL & MANUFACTURING ENGINEERING

NATIONAL UNIVERSITY OF SCIENCES AND TECHNOLOGY

ISLAMABAD

DECEMBER 2019

Experimental Investigation of Energy Harvesting Eel in the Wake of Bluff Body under Ocean Waves

Author

Ehtisham Ali

Registration Number

171615

A thesis submitted in partial fulfillment of the requirements for the degree of

MS Design and Manufacturing Engineering

Thesis Supervisor:

Dr. Emad Uddin

Thesis Supervisor's Signature: _____

DESIGN & MANUFACTURING ENGINEERING

NATIONAL UNIVERSITY OF SCIENCES AND TECHNOLOGY,

ISLAMABAD

DECEMBER 2019

THESIS ACCEPTANCE CERTIFICATE

Certified that final copy of MS thesis written by Ehtisham Ali Registration No.171615, of SMME has been vetted by undersigned, found complete in all respects as per NUST Statutes / Regulations, is free of plagiarism, errors, and mistakes and is accepted as partial fulfillment for award of MS degree. It is further certified that necessary amendments as pointed out by GEC members of the scholar have also been incorporated in the said thesis.

Signature: _____

Name of Supervisor: Dr. Emad Uddin

Date: _____

Signature (HOD): _____

Date: _____

Signature (Principal): _____

Date: _____

Declaration

I certify that this research work titled "*Experimental investigation of energy harvesting eel in the wake of bluff body under ocean waves"* is my own work. The work has not been presented elsewhere for assessment. The material that has been used from other sources it has been properly acknowledged / referred.

Signature of Student

Ehtisham Ali

171615

Plagiarism Certificate (Turnitin Report)

This thesis has been checked for Plagiarism. Turnitin report endorsed by Supervisor is attached.

Signature of Student

Ehtisham Ali

Registration Number

171615

Signature of Supervisor

Copyright Statement

Acknowledgements

I am thankful to my Creator Allah Subhana Wa Ta’ala to have guided me throughout this work at every step and for every new thought which You setup in my mind to improve it. Indeed, I could have done nothing without Your priceless help and guidance. Whosoever helped me throughout the course of my thesis, whether my parents or any other individual was Your will, so indeed none be worthy of praise but You.

I am profusely thankful to my beloved parents who raised me when I was not capable of walking and continued to support me throughout in every department of my life.

I would also like to express special thanks to my supervisor Dr Emad Uddin for his help throughout my thesis. I can safely say that I haven't learned any other engineering subject in such depth than the ones which he has taught.

I would also like to thank Dr. Mushtaq Khan, Dr. Zaib Ali and Dr. Samiur Rahman Shah for being on my thesis guidance and evaluation committee and express my special thanks to them for their help.

Finally, I would like to express my gratitude to all the individuals who have rendered valuable assistance to my study.

Dedicated to my exceptional parents and adored siblings whose tremendous support and cooperation led me to this wonderful accomplishment.

Abstract

A set of experiments are performed in two-dimensional wave flume to investigate the energy harvesting from phase-locked and non-phase-locked modes of vortex in deep water waves by using flexible piezoelectric eel in a controlled oceanic environment. Flapping dynamics of the eel in the wake of circular cylinder at different wave conditions is studied. Energy harvesting potential is examined as a function of streamwise distance from fixed cylinder and spanwise gap along the cylinder at different wave conditions. It is observed that output voltage and eel flapping behaviour are highly dependent on cylinder vortices caused by local wavelength and wave amplitude. Maximum energy is harvested when eel is placed near to the surface caused by high flapping amplitude and frequency. Similarly, at greater depth low flapping amplitude is observed resulting in small output voltage. Maximum output voltages are found at shorter wavelength and at streamwise distance of G_x=1.25 for all spanwise gap along the cylinder and minimum voltages are calculated at longer wavelength and at streamwise distance G_x= 0.75. An increase of 65% in energy harvesting is observed by switching longer wavelength (λ) to shorter one and changing piezo-eel spanwise gap from deep depth to shallow depth. Whereas, an increase of 31.5% was found by keeping wavelength constant and changing spanwise gap of eel. Furthermore, it is observed that energy harvesting from the wake of a bluff body in wavy motion of water is sensitive to the wavelength and wave height. In this study, the effect of wave and geometrical parameters on energy harvesting is studied extensively and proposed that maximum energy harvesting can be achieved by fine tuning of streamwise distance G_x, spanwise gap G_y, wavelength λ and wave height H.

Key Words: *Wave energy harvesting, piezoelectric, energy harvesting eel, fluid structure interaction.*

Table of Contents

List of Figures

List of Tables

CHAPTER 1: INTRODUCTION

1.1 Wave Formation:

All waves start as unsettling influences; the vitality that causes sea waves to frame is known as an upsetting power. A stone tossed into a still lake, for instance, makes waves that transmit out every which way. Arrivals of energy, for example when stone hits the water surface, waves generate. Most of the sea waves are due to the blowing wind on the outer surface of ocean.

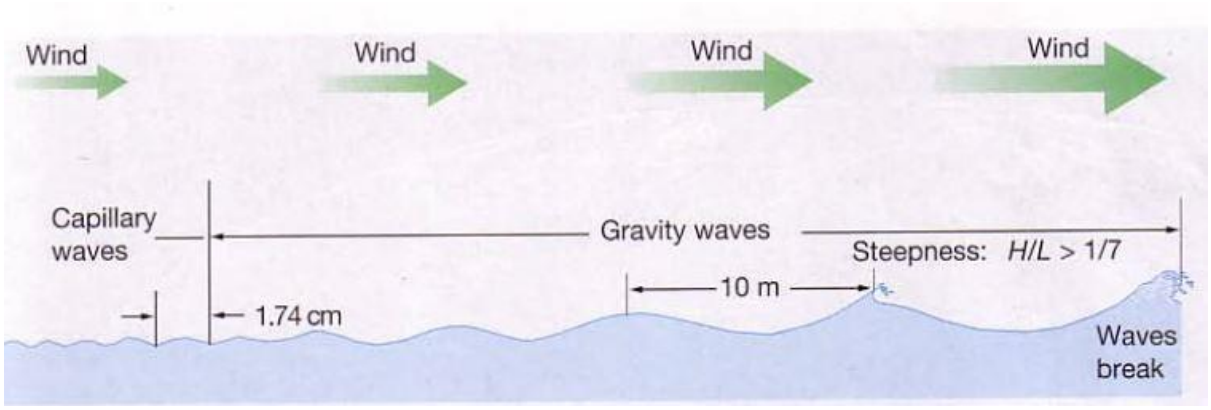

Figure 1: Wind generated wave

The waves transmit out every which way, similarly as when the stone is tossed into the lake, yet on a lot bigger scale. The development of liquids with various densities can likewise make waves. When two different fluid combines, it causes the wave to move. Since ocean and air are both fluid so when they interact with each other, generated wave start moving in the direction of air.

1.1.1 Air-Water interface:

When the air moves on the sea surface it produces turbulence on the surface of the ocean which is the main cause to generate wave.

1.1.2 Air-Air interface:

When air of different densities interacts with each other, their interaction produce turbulence and as a result wave travels. This type of waves are most common when cold air with greater density move towards the warm air with less density.

1.1.3 Water-Water interface:

When water of different densities interacts with each other, waves generates. Since these waves travel beside the limit among waters of various thickness, they are related with a pycnocline. The internal waves can be a lot bigger than surface waves, with statures surpassing more than hundred meters. Tidal development, turbidity flows, wind pressure, or in any event, passing boats at the surface make inner waves, which can now and again be seen from space.

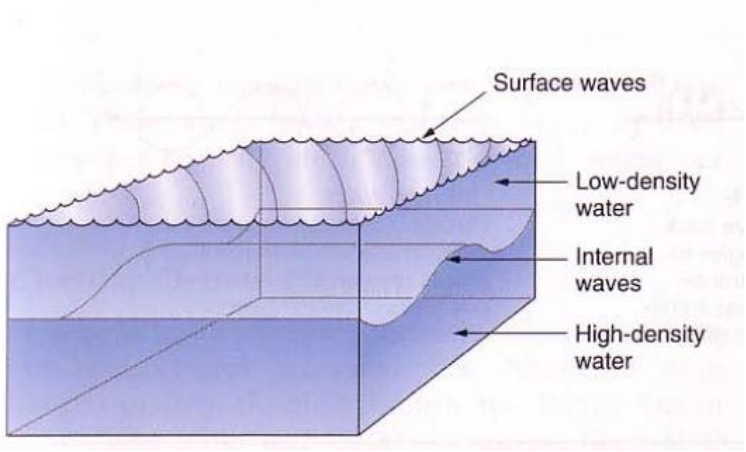

Figure 2: Internal water wave

Mass development into the sea, for example, beach front avalanches or huge icy masses that tumble from seaside ice sheets, additionally makes waves. These waves are ordinarily called sprinkle waves. One more manner by which enormous waves are made includes the elevate or splashing of huge territories of the ocean bottom, which can discharge a lot of vitality to the whole water section. Models incorporate submerged torrential slides (turbidity flows), volcanic ejections, and flaw slippage.

1.2 Wave Motion:

Waves are actually the energy moving from one place to another. The energy travels through waves by the cyclic motion of the particles of the wave. The medium itself doesn't really go in the course of the vitality that is going through it. The medium particles are waver

or cycle, to and fro, all over, or around and around, transmitting energy starting with one molecule then onto the next.

There exist different ways of wave motion. One of the type is progressive waves. Progressive waves are waves that travel by oscillating or vibrating particles in the medium. There are three main types of progressive waves, as mentioned.

1.2.1 Longitudinal wave:

Longitudinal waves are progressive waves in which particles vibrate parallel to the wave motion. Example of longitudinal wave is the motion of spring in which its coil compress or expand in the direction of energy travel. These types of waves can transmit energy in any field of matter i.e. gases, liquid and solid.

1.2.2 Transverse waves:

In transverse waves, energy goes at right edges to the heading of the vibrating particles. Most of the energy through solid travel by transverse waves because in solids molecules are bound to each other and unable to make high amplitude vibration.

1.2.3 Orbital Waves:

In orbital waves, particle motion consists of both components of longitudinal and transverse motion. Due to transverse and longitudinal motion at the same time, particles start moving into circular orbit, formed orbital wave. The waves which transfer energy via body of the medium are called body waves like longitudinal and transverse waves. Similarly, orbital waves are also a body waves because it transfers energy via surface of the ocean which is in contact with atmosphere. Ocean waves are orbital in nature hence in this paper, orbital waves are used for ocean waves.

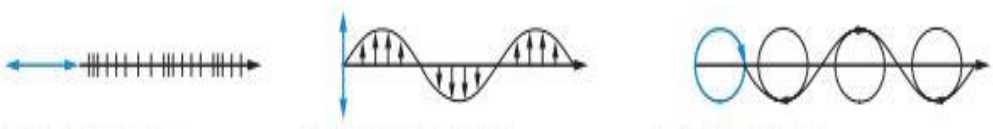

Figure 3: Types of progressive waves 1) Longitudinal wave 2) Transverse wave 3) Orbital wave

1.3 Types of Ocean Waves:

There are many sources which causes waves in the ocean. But mostly, wind is the major cause of generating waves called wind generated waves. Still there exist other sources of wave generation which produce different types of waves like tsunami, tidal waves, internal waves, human induced waves and splash waves. Major categories are explained as under.

1.3.1 Wind waves:

Wind waves are produced due to the motion of wind over the free surface of the ocean, river or canal. These types of waves travel a large distance and have a time period range from 0.1 sec to 5 minutes. Wind waves are generated due to disturbance in the shear layer by wind blowing which caused ripples to form. These ripples get more energy from the waves and converted into fully developed wave of specific wave height and wavelength. Wind waves or simply called the surface waves consist of large portion of the ocean wave energy.

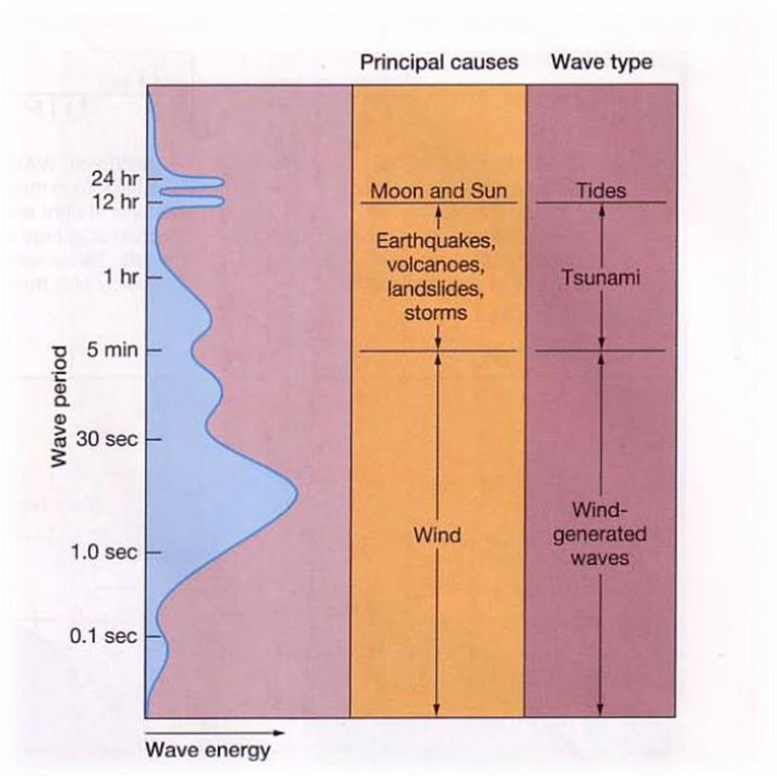

Figure 4: Ocean wave energy distribution

1.3.2 Tsunami:

Tsunami waves formed due to the large portion of water movement. The major reasons of the tsunami include, earthquakes, explosion underwater, large lake or volcanic ejection.

Tsunami waves are different from the normal surface waves in the sense because these waves have large wavelength which results in large destructions.

1.3.3 Tides:

Tidal waves are formed due to the gravitational pull of moon and sun and earth's gravity act as restoring force. These waves have larger wave period ranged from 12 hours to many hours depending on many factors. Tidal energy can also be harvested but it requires high cost and huge structure.

1.4 Wave Characteristics:

Characteristics of ocean waves are different for different types of waves. In this paper only surface gravity waves have been considered. An ideal wave has a profile like a sine curve, so it is also called a sine wave.

1.4.1 Crest and trough:

High parts of the moving wave are called crest. Similarly, low parts of the wave are called trough.

1.4.2 Zero energy level:

The mid points of crest and trough are called zero energy level or still water level. This point indicates the original water level when there is no wave present.

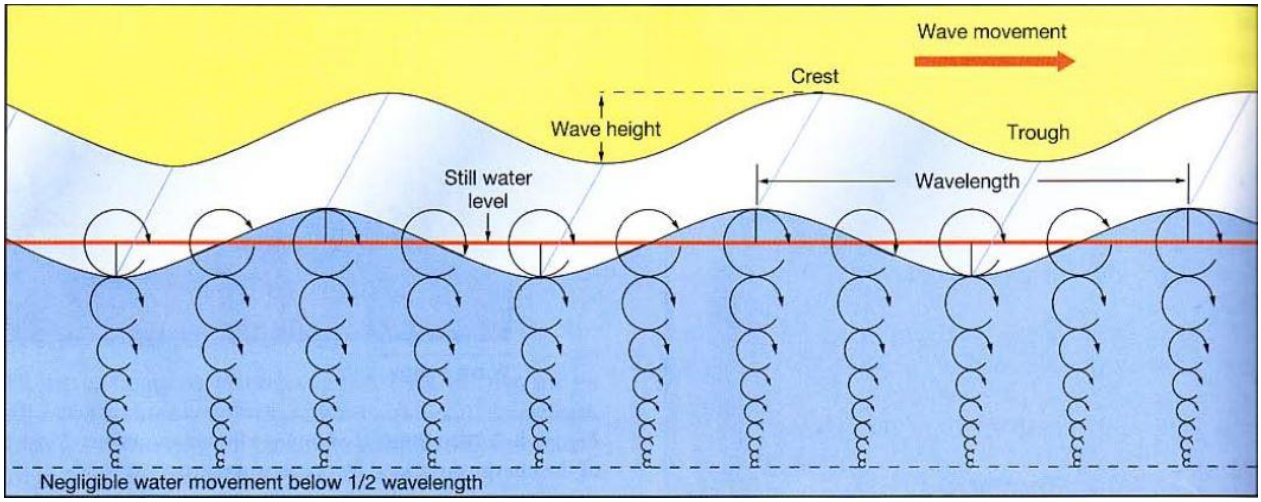

Figure 5: Ocean wave characteristics

1.4.3 Wave Height:

It is the vertical distance from high points of the wave to lower points of the wave and is denoted by symbol H and can be measured by visual way or using wave gauges.

1.4.4 Wavelength:

The horizontal distance from consecutives lower points or higher points is called wavelength and is denoted by L and represented in fig.

1.4.5 Wave steepness:

Wave steepness can be expressed as the ratio of height of the wave to the wavelength.

$$\text{steepness} = \frac{Wave\ height\ (H)}{wavelength(L)}$$

Wave steepness is very important factor because it provides the maximum height achieved for a same wavelength. when this ratio exceeds 1/7 then wave will break and its height decreases. So, to harvest maximum energy from wave, steepness ratio must be lower than 1/7.

1.4.6 Wave Period:

It is the time required by the wave to complete one wave or time taken by wave crest or trough to pass from the same point and is represented by T.

1.4.7 Wave Frequency:

It is the total number of waves passing through fixed point in one second and is represented by f. Wave frequency is the reciprocal of the wave period.

$$f = \frac{1}{T}$$

1.4.8 Circular Orbital motion:

During the wave travel water does not move along the wave but the energy moves. When the wave move, the particles of the medium moves in a circular motion rather than

unidirectional motion. This development is called circular orbital motion. Perception of an article coasting in the waves uncovers that it moves not just here and there, yet additionally marginally forward and in reverse with each progressive wave. Due to this circular motion, water particle forced forward, upward and backward again to attain its initial position while transferring energy to the consecutive particle.

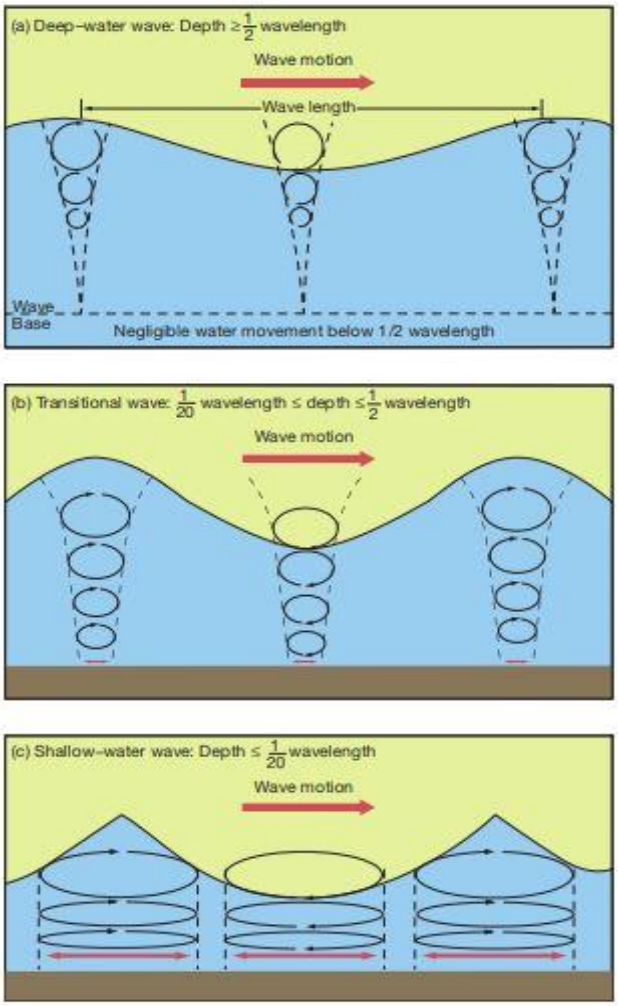

Figure 6: Comparison of a) Deep water wave b) Transition wave and c) Shallow water wave

1.4.9 Wave Base:

Near to the surface, diameter of the orbital motion of wave particle is equal to the height of the wave. But as depth increases, particle orbiting diameter decreases gradually and at a specific depth when it is equal to half of the wavelength, motion of the particle become unaffected by wave motion. This depth is referred as wave base. Ocean waves can be categorized depending on the depth of wave base as mentioned.

1.4.10 Deep Ocean Waves:

If depth of water is greater than the half of the wavelength (wave base), wave formed are deep ocean waves. Deep ocean waves have no interaction with ocean bed. Mathematically we can write as

$$\text{Water depth} > \frac{L}{2}$$

As water depth is larger so celerity of the deep ocean waves only depends on the wavelength and can be calculated as

$$S = \frac{Wavelength\ (L)}{Time\ period\ (T)}$$

By putting gravitational value, we can rewrite celerity as

$$S = 1.25\sqrt{Wavelength}$$

This equation shows that when the wavelength is large, speed of the wave increases.

1.4.11 Shallow Ocean Waves:

If the water depth is less than $1/20^{th}$ times of the wavelength, waves formed are called shallow water waves. Mathematical expression is given by

$$\text{Water depth} < \frac{L}{20}$$

As depth is very less than wavelength, wave particles fells the ocean bed and its celerity depends on gravitational force as well as water depth and can be expressed as

$$S = 3.13\sqrt{Depth}$$

1.4.12 Transitional ocean waves:

These types of waves have characteristics of both deep ocean waves and shallow ocean waves. These waves produced when water depth is between 1/2 to $1/20^{th}$ times of the wavelength. Celerity of the transitional ocean waves is a function of water depth and wavelength.

CHAPTER 2: LITERATURE REVIEW

2.1 Mechanical Wave Energy Converter

An ocean wave energy gatherer from the horizontal component of wave movement of water particles is created [12]. The gatherer comprising of a beam substrate appended by piezoelectric devices and a resilient mass is utilized to gather output energy inferable from the electromechanical combination influence of the piezo devices from the horizontal wave movement [15]. To harvest the energy from piezoelectric device, a numerical model presents the output charge and obtained voltage from piezo device using direct wave hypothesis and flexible bar model. According to collected results the produced power increased with increase in the width of the cantilever by increasing width to thickness ratio, the wave stature, the ocean profundity, by increasing the proof mass over cantilever mass, and the proportion of the ocean profundity to the length of the wave. Energy harvesting of 55 watts has been approximated for a specific wave height, wavelength [22]

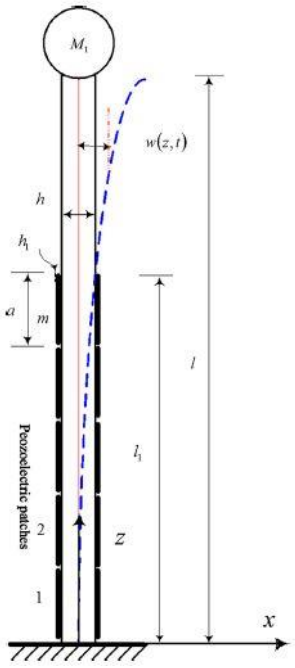

Figure 7: Schematic representation of experimental setup [12]

Output RMS power was calculated for different parameters including, wave height, wavelength, depth, thickness to width ratio and proof mass. It was observed that the output

power increased as wave height increased as shown in the figure. When proof mass amplified, the power output also increased due to increase in inertial effect [17].

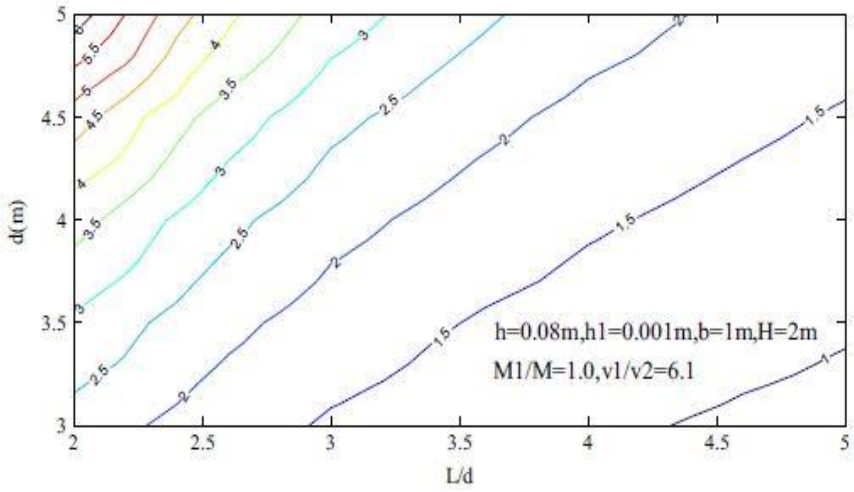

Figure 8: Output RMS as a function of wave height, wavelength, depth and mass ratio [17]

In this test, the mechanical energy is converted into electrical energy when the sea wa ves crashes into a vertical face. To do this, an incredible energy reaping frame segment piezoelectric bar volume failure is suggested [24]. A conceptual model is presented and logically analysed to understand the use of this system. The logical model is refreshed utilizing exploratory information and it is indicated that the explanatory outcomes were like the test results in the wake of refreshing. In the wake of approving the electromechanical model, an energy gathering framework is introduced, which can deliver energy from breaking sea waves on a vertical face [26]. Four potential reasonable plans for energy collecting frameworks are considered and the supposed Perfection Rate (PR) is acquainted with select the best model to expand reaped energy while alleviating the breaking down impacts of enormous strain twisting.

The test refreshed outcomes and utilize a numerical model of the energy reaper that is created to clarify the activity of the gadget after approval. So as to expand the collected energy, the conduct of four potential designs was explored.

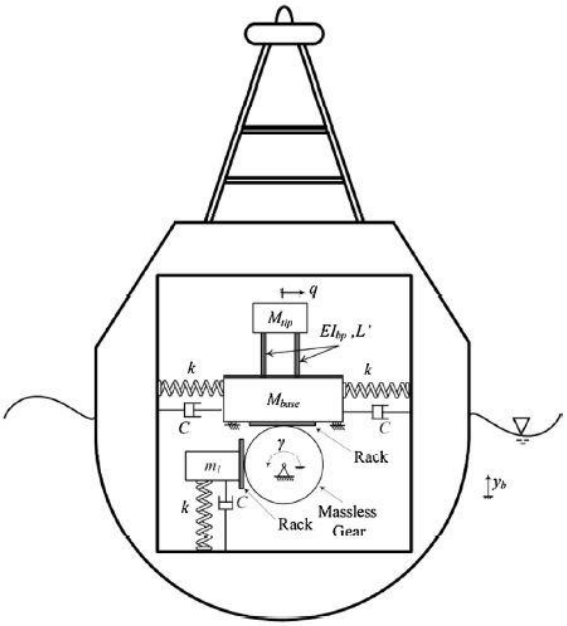

Figure 9: Schematic representation of ocean buoy energy harvester system [26]

As far as energy collecting, a reasonable model is actualized to diminish the size of energy collectors to incorporate a bar section piezoelectric energy reaper that can work in a double recurrence space [27]. To consider both the life expectancy of the structure and the collected energy, the alleged Perfection Rate is presented [32].

A lift based orbital wave energy converter is explored in down scale two-dimensional wave flume try [33]. This sort of wave energy converter comprises of a pole with one or more hydrofoils appended unconventionally at a span. The principle shaft is adjusted parallel to the wave peaks and submerged at a fixed profundity [35]. The activity of the converter both as a wave generator just as a wave-to-shaft energy converter connecting with straight peaked waves is illustrated. The geometry of the converter is demonstrated to be reasonable for wave end of straight peaked consonant and sporadic waves. The effect of structure parameters, for example, gadget size, submergence profundity, and number of hydrofoils on the exhibition of the converter is appeared. For ideal parameter decisions, trial results show energy extraction efficiencies of over 95% of the approaching wave energy [37]. This is accomplished utilizing input control to synchronize the pivot of the wave energy converter to the approaching wave and altering the cutting edge contribute edge extent to the wave tallness. Because of the capacity of the converter to produce a solitary sided wave with not many consonant waves, little energy is lost to waves transmitting in the up-wave and down-wave bearings [38].

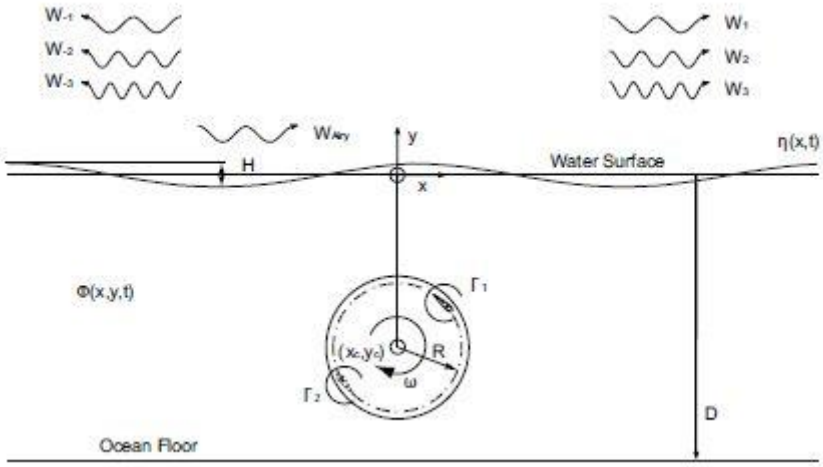

Figure 10: Cycloidal wave energy converter [37]

In this investigation, the world's first movable sea dynamic energy reaping framework utilizing ionic material was created and applied to the transformation of the active energy of the sea into power [38]. The framework was reproduced to assess its development and basic solidness and to recognize the arrangement that would advance its energy collecting execution. Tests under genuine ocean conditions were likewise performed to evaluate the electrical gathering execution of the ionic material framework.

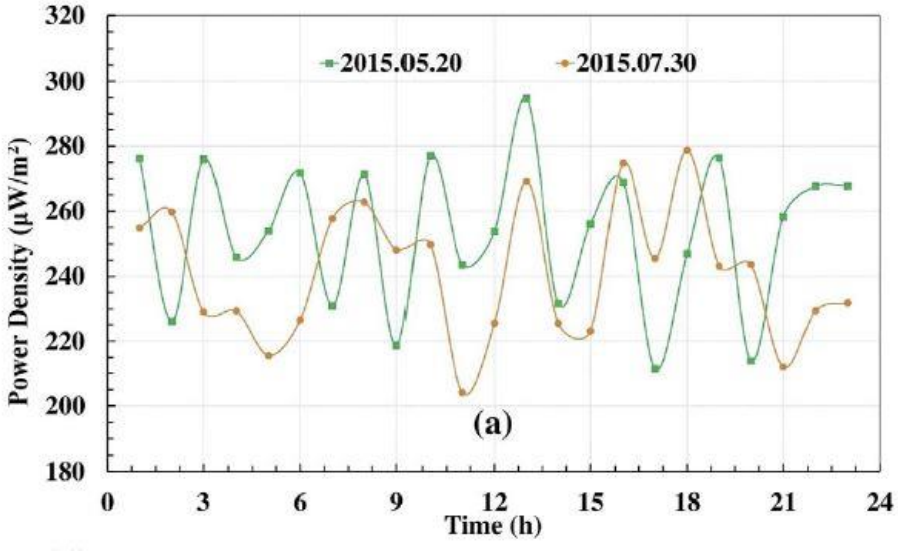

Figure 11: Output power as a function of time [38]

When all is said in done, the revolution of the modules is little: the normal adequacy of the 18 modules in the move, pitch, and yaw motions is just around 1° at a recurrence of 0.48Hz.

What's more, the z-uprooting is noteworthy higher than the adequacy of the episode wave and other course relocations. The test results indicated that the normal control thickness at a given time unequivocally wavered over 180 μW/m2, with a normal power thickness of roughly 245 μW/m2 and a pinnacle estimation of 292 μW/m2 [44]. For the most part, the power thickness of the IPMC framework is a lot littler than that of conventional energy sources; in any case, ionic polymer is a modest also, sturdy material and the intensity of the framework can along these lines be improved by expanding the dynamic region of ionic polymer.

2.2 Piezoelectricity

As the name suggests the piezoelectric materials voltage in response to the pressure or stress applied on them. These materials generate electric current as the deformation is produced in them as a result of stress. Their study was only confined to the electric current generation form the deformation of the piezoelectric material which is called direct piezoelectric effect. Another effect of piezoelectric material was discovered by the French scientist name Garbriel Lippmann. He discovered that the piezoelectric material undergoes deformation under the influence of external electric charge. The mathematical argument regarding this was experimentally proved and concluded in the same year by [7].

In their work the Curie brother studied the naturally existing Quartz crystals. They concluded that the main reason behind generation of electric current from naturally existing piezoelectric material is the formation of natural dipoles within the material. This is the main phenomena which are applied to all existing piezoelectric materials. The formation of dipoles varies differently according to specific category of the material [9].

After determining that electric dipoles generate electricity, we can determine that how direct and inverse piezoelectric effects are produced. We can determine that how different parameters have effect on the piezoelectric energy generating capability of the material. The piezoelectric material is electrically neutral in the absence of stress and deformation which means that both the positive and negative electrode in the material are coinciding with each other. When the stress or pressure is applied on the filament the centers of positive and negative electrodes get stretched or compressed creating a field of current with in the material and generating the voltage difference. The conductive wire is connected to positive and negative electrodes of the material in order to transmit charge from material to external circuit. This is basis of direct piezoelectric effect of the piezoelectric material. Contrary to this concept an

externally applied electric field has an impact on the neutral behavior of a piezoelectric material.

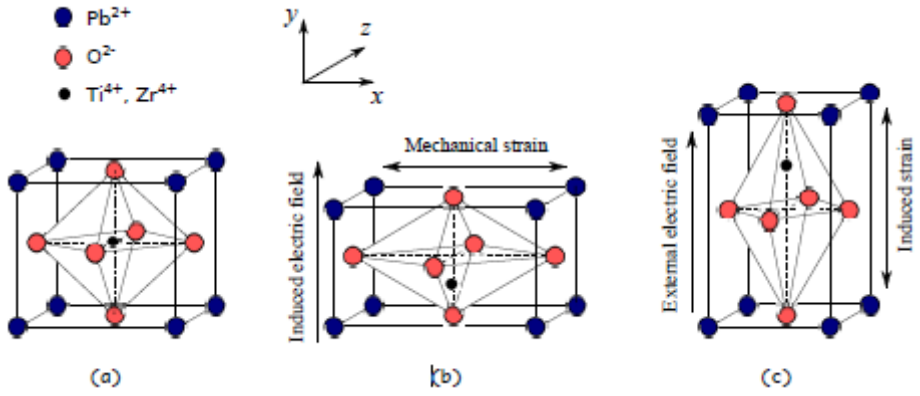

Figure 12: a) Cell Structure of piezoelectric material b) direct piezoelectric effect c) Inverse piezoelectric effect

The electric field will change the internal electrical dynamics of the piezoelectric material. In order to restore it original position and thus neutrality of the piezoelectric material the positive and negative electrode move in such a way that they come to their originally neutral positions, thus the material is mechanically deformed and stress in induced in the system producing inverse piezoelectric effect.

Consider the elementary crystal of piezoelectric crystal lead zirconate titanate (PZT) as shown in figure 3. The figure 3(a) shows the crystal in neutral form i.e. the positive and negative electrodes of the crystal are at center and same point. As the strain is applied on the structure figure 3(b) the centers of the crystal move away from each other in the vertical direction and generate the electric field which can be transmitted to external circuit. On the contrary if external electric potential is applied on the PZT crystal as shown in figure 3(c) the positive and negative electrodes move opposite to each other causing deformation inside the structure.

There are many four categories of piezoelectric materials that are described below.

2.2.1 Ceramics

The piezoelectric ceramics have excellent piezoelectric properties. The main advantage of piezoelectric ceramics is that they are made in the powder form and thus can be transformed into any type of geometric shape like disc, cylinders, plates or thin films. The piezoelectric properties of quartz are stronger than ceramics but conforming into any shape is considered

very advantageous for ceramics piezoelectric materials. As they are ceramics with high brittleness, so their application is also limited

2.2.2 Quartz

This is the naturally occurring kind of piezoelectric material and is in the form of crystals. It has strong piezoelectric properties along with high stiffness, low sensitivity to temperature and atmospheric conditions. These are used where more precision is required like in frequency control modules, electronic watches and microprocessor-based equipment. They are less applicable to be used in places where high deformation is required. They cannot also be shaped into different shapes owing to their crystalline properties.

2.2.3 Polymers

Mostly used piezoelectric material is PVDF polyvinylidene Fluoride. Polymers have natural properties that they are very flexible in nature and are softer as compared to quartz and ceramics. They have weak piezoelectric properties but due to their flexibility they are used in variety applications. They are more mechanically stable as due to their flexibility. They usually come in the form of thin filaments and can be transformed into desired lengths. Due to ability to sustain large deformations they are widely used in experimental research work regarding energy generation from piezoelectric materials.

2.2.4 Composite materials

The flexibility of polymers and rigidity of ceramics is incorporated is special type of piezoelectric material that are softer and flexible and at the same time have certain kind of rigidity. Due to these structural properties the composite piezoelectric material can be used in the studies where large deformation is required.

2.3 Piezoelectric Energy Harvester:

To power small electronics, such as weather monitoring, wave monitoring, temperature sensors and vibration sensors etc, piezoelectric devices have been extensively used as a energy source. Much research has been done to harvest energy from piezoelectric devices due to its simplicity and low cost. Research has been done to harvest energy from piezoelectric flexible device when it is placed in the wind, water and vortices [42]. The design and performance of piezoelectric devices for different application has been done [44]. Several mathematical model

and numerical techniques have also been studied [50]. Energy harvesting from piezoelectric can be categorized into three main types, energy harvesting from wind flow, energy harvesting from water flow and energy harvesting from ocean waves.

2.3.1 Piezoelectric Energy Harvesting from Wind Flow:

Much research has been done to harvest energy using piezoelectric from wind using fluttering, vortex induced vibration and galloping. Piezoelectric flag flapping in the flow induced vibration is a very common phenomenon.

a) Energy Harvesting from VIV:

Hobbs harvested the wind energy using vortex induced vibration of vibrating cylinder and investigated its performance by altering flow speed and cylinder distances [42]. Weinstien harvested energy from VIV with turbulent air flow [47]. Gao et al harvested wind energy using piezoelectric cantilever of cylinder [33]. Die at al presented a theoretical model to harvest wind energy using cantilever of cylinder [39]. Akaydin et al investigated the wind energy harvesting using vibration produced by flexible piezoelectric structure [44].

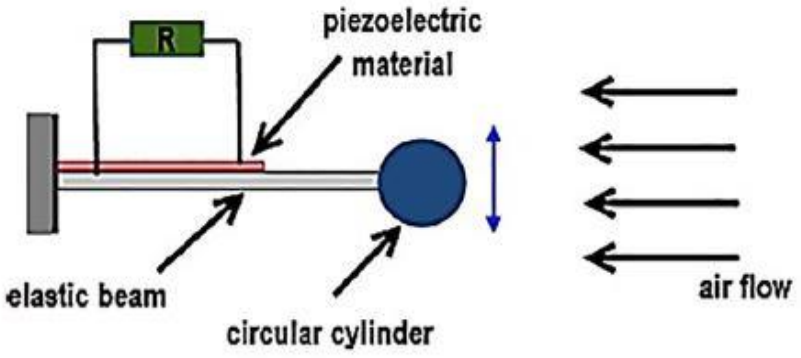

Figure 13: Vortex induced vibration [42]

Dunnmon harvested wind energy in the wake of bluff body using piezoelectric flag and investigated its performance for different parameters [27].

b) Energy Harvesting from Turbulent Layer:

Much research has been done to harvest wind energy from turbulence created by the wake of different bluff bodies and vibration induced due to the wind flow. Akaydine investigated the experimental energy harvesting when piezoelectric flag was placed in the wake of circular cylinder [29]. He also tested energy harvesting efficiency for different Reynold numbers. Goushcha present the study of energy harvesting using turbulence produced by the shear layer of wind [28]. Mathematical model and simulation also have been done to predict output energy caused by vibration and shear turbulence by the wind in the wakes of bluff body.

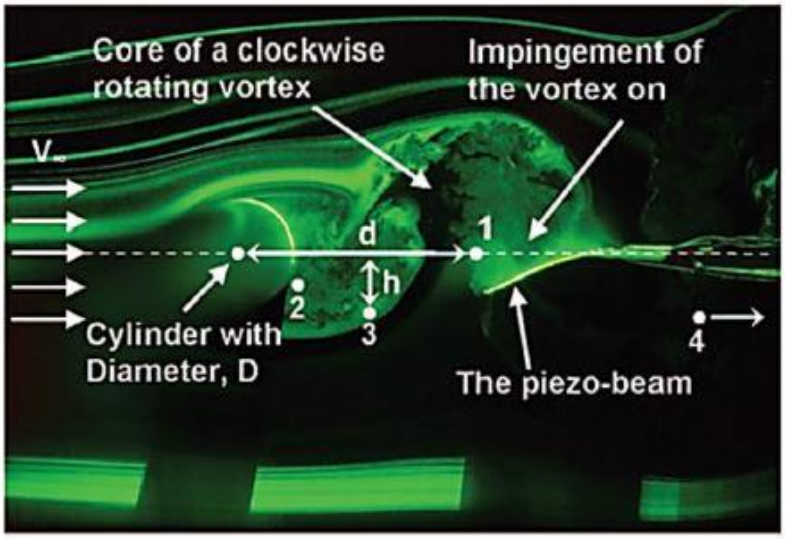

Figure 14: Energy harvesting film from wind shear layer [29]

c) Energy harvesting from fluttering:

Periodic motion produced by the aerodynamic force cases fluttering in the structure. Energy harvesting has been investigated by fluttering vibration in the wind flow [31]. From the energy reaping perspective, the piezoelectric energy reaping gadget is situated in a stream field also, eager to experience huge utmost cycle swaying, which could be changed over into the electrical energy; along these lines, the stream speed has a significant effect on the presentation of the piezo-aeroelastic frameworks.

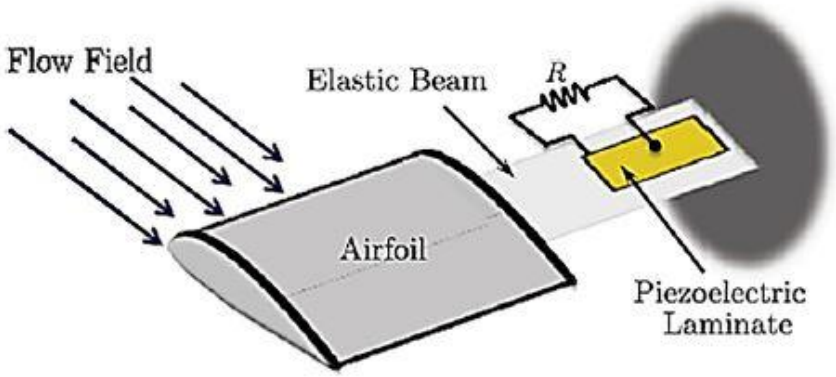

Figure 15: Energy harvesting from wind fluttering [31]

2.3.2 Piezoelectric Energy Harvesting from water flow:

A lot of research has been done to harvest energy from the deformation of the piezoelectric device placed in the water flow. The installation of energy collectors in the pipeline could be used as small scale energy harvesting device [32]. Hence, energy gatherer gadgets with piezoelectric methods have been created for the inner liquid stream. In such manner, numerous examinations have been done on energy reaping dependent on the utilizing of the piezoelectric materials in liquid stream in channels. Lee et al utilized a piezoelectric stream energy gathering gadget, containing a cantilevered transducer with one or a few piezoelectric material layers appended to its surface [41]. Due to the motion of the water, the vibration in the piezoelectric device produced the energy which is harvested and could be used to power electronics that require millivolts for its operation.

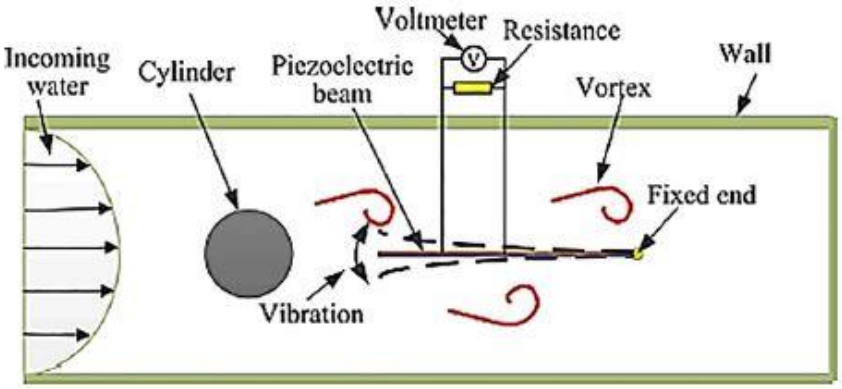

Figure 16: Schematic representation of energy harvesting from water flow in the wake of bluff body [41]

2.3.3 Piezoelectric Energy Harvesting from Ocean Waves:

In recent past, much research has been focused to harvest ocean wave energy due to its distinctive characteristics of concentrated, high power density and widely available renewable energy but it is still lag due to its high cost and high maintenance requirements. Researcher has investigated the experimental study of energy harvesting using array of piezoelectric flexible device when placed transversally and vertically to the orbital motion of the ocean wave [17].

2.4 Bluff body wakes:

2.4.1 Bluff Body Wakes in uniform flow:

Kim and lee has studied the wakes of different geometry bluff bodies (circular, rectangular, square, D shape and triangular) at different Reynolds [49]. Wakes of circular cylinder is simple as compared with other non-circular cylinders. However, vortices were found continuous, stronger and more effective for triangular cylinder resulting in a good bluff body at all.

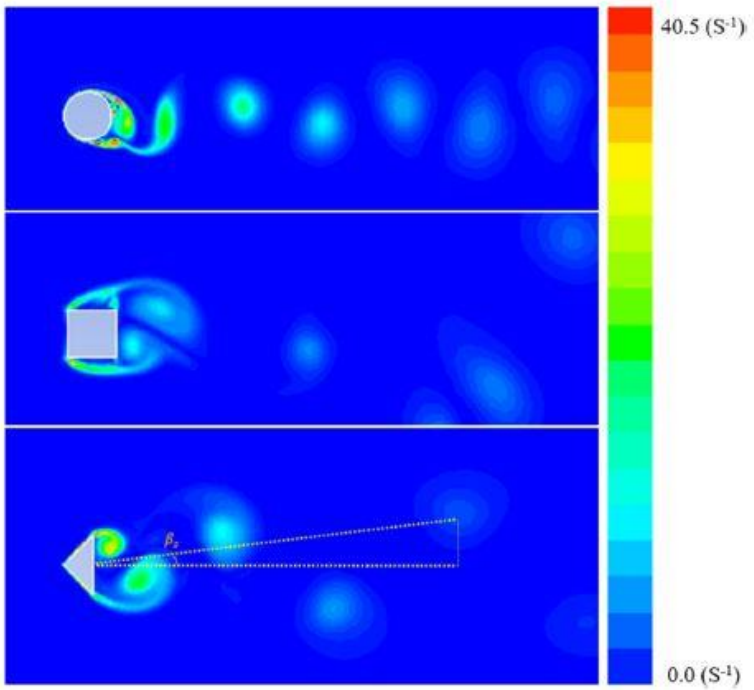

Figure 17: Wake region for circular, square and triangular bluff body [49]

2.4.2 Bluff body wakes under waves:

Most researcher had performed PIV to study wakes around a horizontal circular cylinder in uniform flow [26] and [29]. They had performed Numerical simulation for waves and circular cylinder interaction. Young had studied the interaction of deep water waves with fixed vertical cylinder and operated particle image velocimetry to investigate the wake behaviour spanwise to the cylinder for different wave conditions [33].

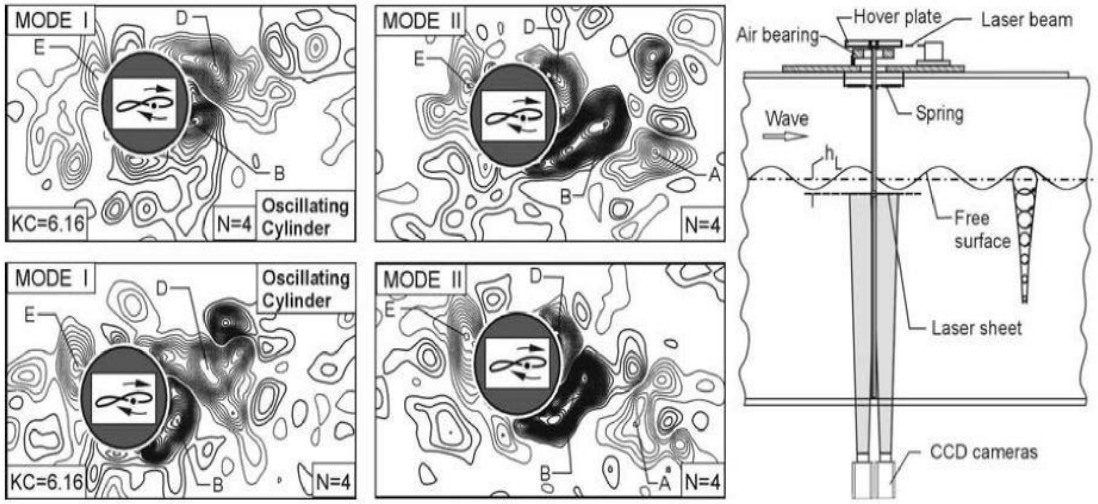

Figure 18: Schematic arrangement and wake region for cylinder under waves [29]

The experimental study of water waves interaction with vertical circular cylinder has been demonstrated [30].

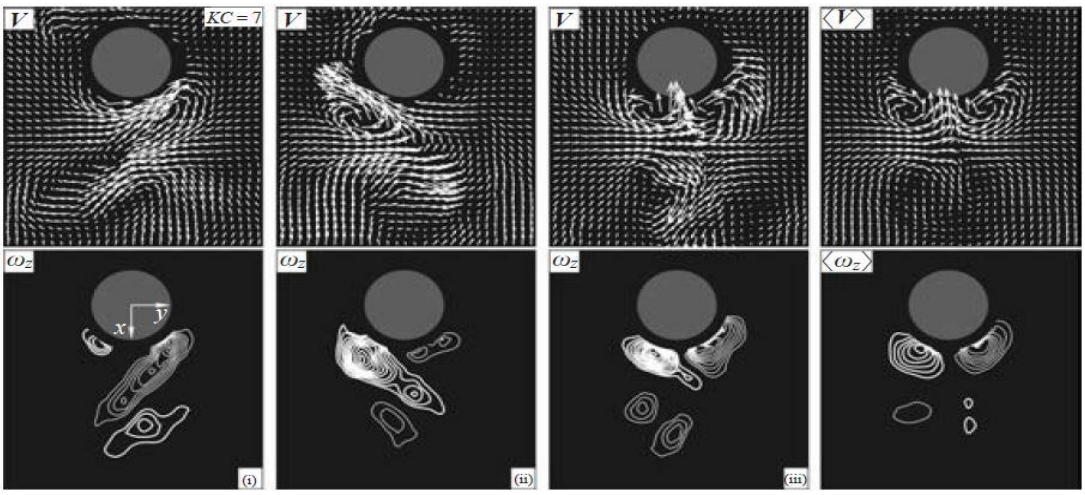

Figure 19: PIV result of cylinder vortices at different wave conditions [30]

2.5 Water particles trajectories under waves:

Et al has studied the trajectories of water particle for surface gravity waves visually in experimental flume and their affect with depth below the free surface [40]. It was observed that near the surface, particle orbital motion was circular but at depth magnitude of orbit decrease and horse-shoe motion of the particle was observed.

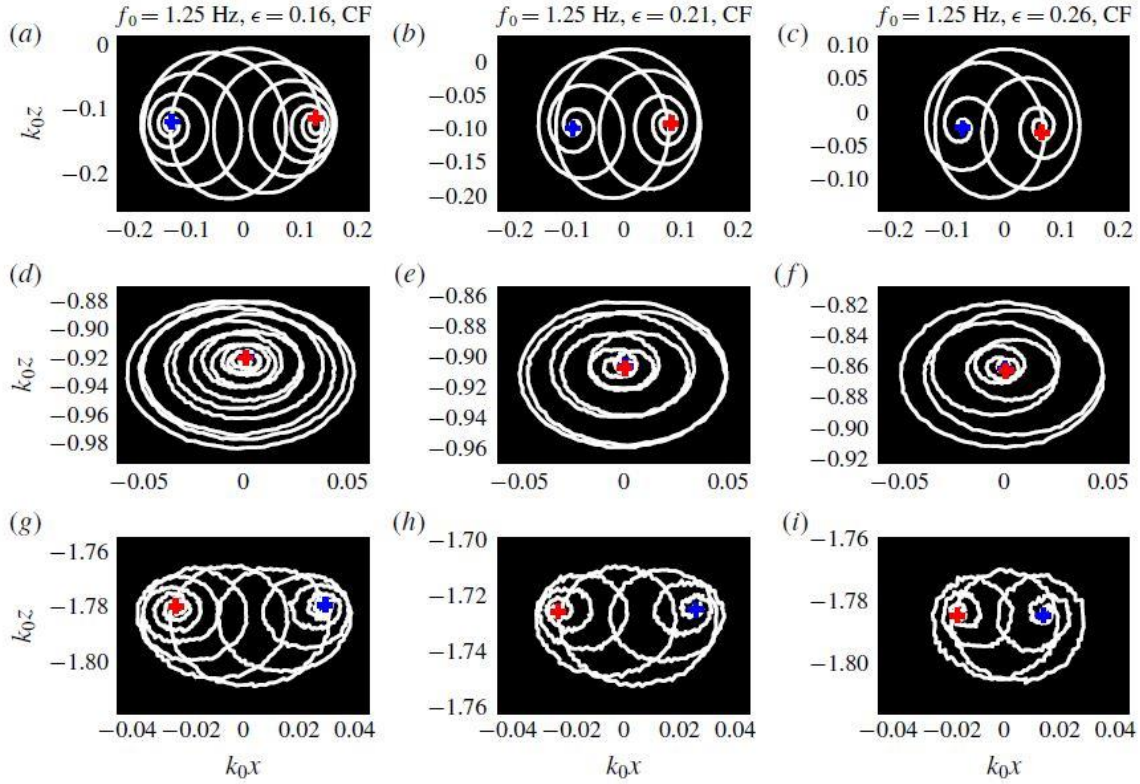

Figure 20: Particle trajectories at different water depth [40]

CHAPTER 3: WAVE GENERATOR

Wave generator are used to generate the different types of ocean waves in the laboratory flumes including deep water waves, shallow water waves, tsunami and tidal wave.

There are many different types of wave generator used in the experimental flumes depending on the characteristics of the wave tank i.e. its length, width and height. There are two major types of wave maker used in the experimental wave tanks.

3.1 Flap type wave generator:

Flap wave generators are utilized to deliver profound water waves where the orbital molecule movement rots with profundity and there is immaterial movement at the base. Commonplace applications are demonstrating skimming structures in profound water and exploring the material science of sea waves. Frequently the pivot of the oar is mounted on an edge some separation over the tank floor.

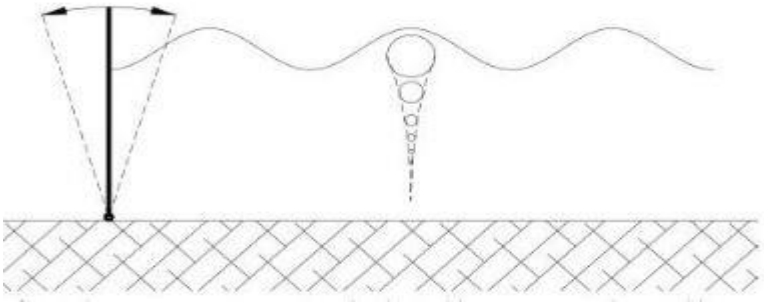

Figure 21: Schematic representation of flap type wake generator

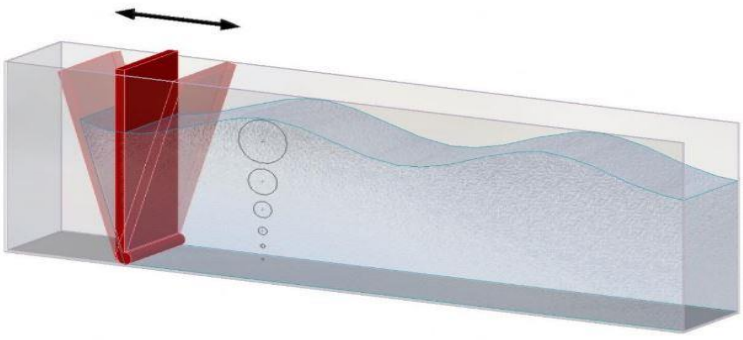

Figure 22: Flap type wave generator 3D view

3.2 Piston Wave Generator:

Piston type wave generator are used where shallow ocean waves are required and the water depth is very less than the wavelength. At the surface, orbital movement is circular, and it becomes elliptical when moving into the deep water. At the ocean base, particles are affected by waves and moves in a linear way rather than unaffected as in deep waves.

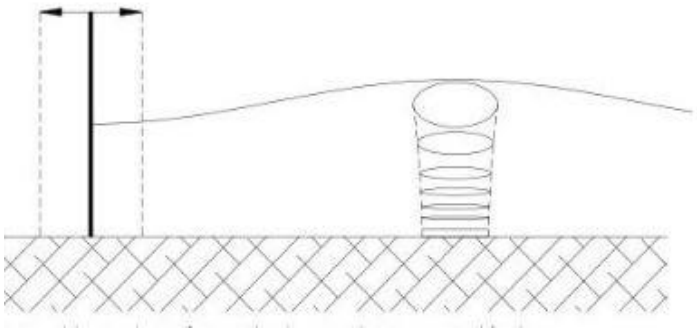

Figure 23: Schematic representation of piston type wave generator

All oars will have an ideal recurrence where the flat movement is near the movement of the water. This is where the idleness of the water, or included mass, is most minimal. As the recurrence is expanded the crisscross between the oar and the water movement makes the additional mass increment. This impact can be found in a wave tank where a piston wave maker produces high repetition waves, despite the fact that the movement is little, the oar moves a square of water that seems, by all accounts, to be appended to it. High frequencies don't require high power yet can apply high inertial loads on the structure. At low frequencies the volume dislodged by as far as possible the wave stature. Piston moves double the water as compared with flap type wave maker in every stroke so the wave will be roughly twice as large. Despite the fact that the heaps are low the plan centre turns into the oar stroke and counteracting spillage round the structure.

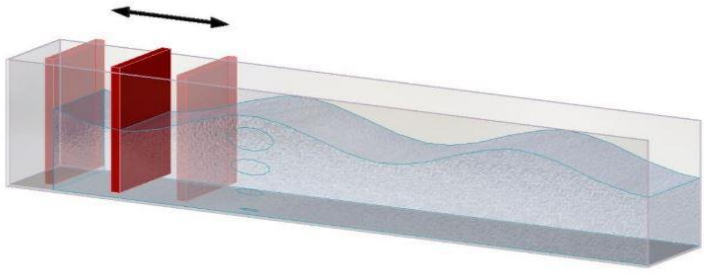

Figure 24: Piston type wave maker 3D view

CHAPTER 4: WAVE ABSORBER

Wave absorber plays a very important role to overcome wave reflection in the experimental wave flumes. Efficiency of wave absorber can be categorized based on the wave reflection coefficient C. Reflection coefficient C is defined as the ratio of incident wave height to the reflected wave height.

4.1 Standard Sloping Beach:

This wave absorber is the ordinary wave absorber that is utilized in a large portion of the wave flumes and bowls far and wide. The safeguard comprises of a basic straight incline. Various materials are utilized, however generally this safeguard is developed out of granular material. The general guideline of this wave absorber depends on the scattering of wave vitality because of wave breaking brought about by the lessening water profundity.

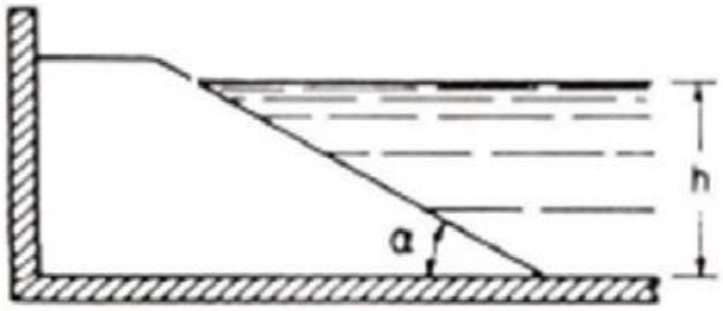

Figure 25: Standard sloping beach

4.2 Sloping Beach without Bottom:

The distinction between this wave absorber and the standard slanting seashore is that the slant is cut off at a specific profundity underneath the still water level as shown in fig. A first favourable position of this absorber is that less material should be expended. The expansion of the reflection coefficient because of the way that the incline doesn't arrive at the base any longer is by and large little. The vast majority of the wave vitality is in reality arranged near the still water level, where the wave proliferates, and here the slant is available to scatter this vitality. All things considered, one goes to the most fascinating bit of leeway of this wave absorber, to be specific the way that at the most significant territory, for example near the still

water level, a littler incline can be utilized than an identical standard slanting sea shore taking a similar space in the office. This should bring about a superior presentation of the inclining seashore that doesn't arrive at the base as for its identical standard inclining seashore.

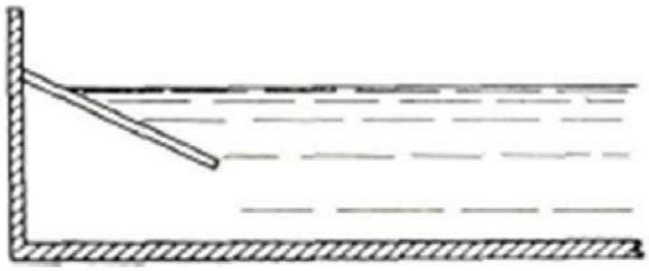

Figure 26: Sloping beach with no bottom

4.3 Sloping Beach with Mesh:

This wave absorber takes after a lot to the standard slanting seashore yet for this situation a mesh is put in front of it. This mesh has the goal to scatter effectively some wave vitality before the waves arrive at the seashore. Be that as it may, on the off chance that one needs to keep up a similar all out length as a standard inclining seashore, the seashore should be made more extreme. In the event that the mesh can make up for the loss of proficiency cause by this, this wave absorber will perform superior to a standard slanting seashore. In the event that this isn't the situation, in any case, the standard inclining seashore will perform better.

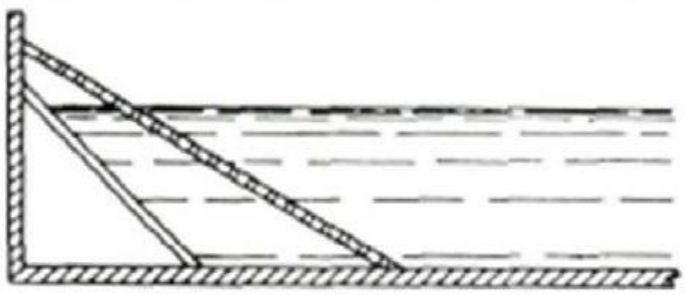

Figure 27: Sloping beach with mesh

4.4 Split Slope:

This wave absorber has a more extreme slope at higher profundities furthermore, a milder slope nearer to the still water level as it shows in Figure. In that capacity the littler slope is present where the wave vitality is the most elevated and as a result the waves will be damped more than a standard inclining seashore with a similar length would sodden them. Assuming,

be that as it may, the water level is situated underneath the wrinkle in the slope, where the slope is more extreme, this wave absorber is less effective. This is a detriment of this wave absorber regarding the inclining seashore that doesn't arrive at the base that, if the situation of the slope is caused customizable, to can be utilized productively at various water levels.

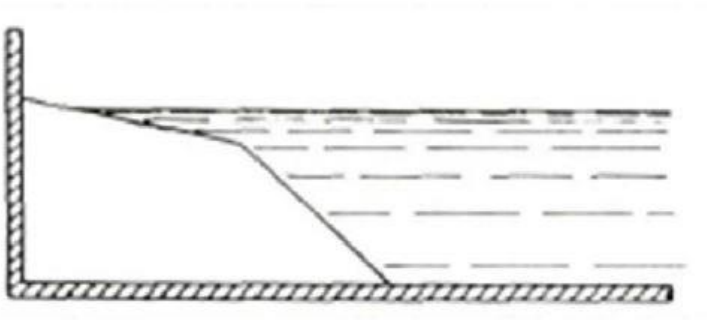

Figure 28: Split slop wave absorber

4.5 Split Slope without Bottom:

This wave absorber does, much the same as the standard beach without bottom, not arrive at the base of the wave flume or wave bowl. Nonetheless, interestingly this prior examined absorber this wave absorber doesn't have a steady slope however a slope develops out of three various parts. The most reduced part is the least significant as the wave vitality is the most reduced there. Along these lines, this part has the most elevated steepness. The piece of the slope in the centre has a lower steepness as it is progressively significant and the upper part, which is situated in the area of the still water level, where the wave vitality is the most elevated, has the least steepness, as it is the most significant part. Due to the way that this absorber doesn't arrive at the base, its situation can be made customizable, which makes it proficient at various water levels.

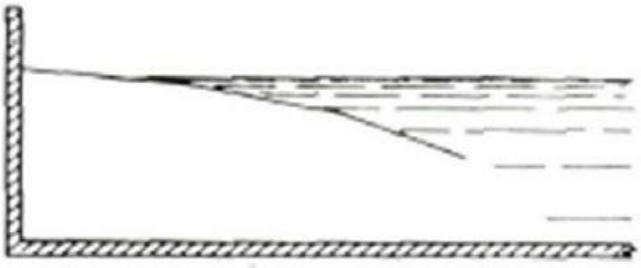

Figure 29: Split slop with no bottom

4.6 Slope with Vertical Wall:

This wave absorber is fundamentally the same as the wave absorber that doesn't arrive at the base. Be that as it may, one can see in Figure that the slope of this wave absorber is associated with the base by a front divider. This causes the wave absorber to be fixed. As an outcome, it will just be proficient for water levels, which are higher than the tallness of the front divider. This is a impediment regarding wave absorber that doesn't arrive at the base, however in the event that the architects realize that no tests will be completed in the office with water levels lower than (or in the outline of) the stature of the front divider this wave absorber can be utilized and no framework to make the situation of the slope flexible is important.

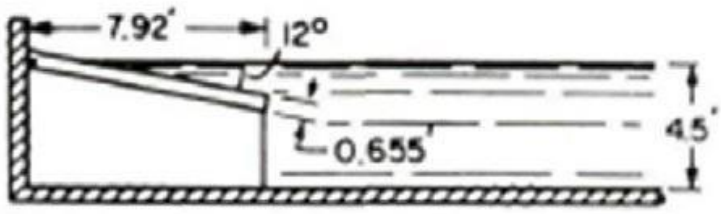

Figure 30: Slop with vertical wall

4.7 Marcou Wave Absorber:

This wave absorber can in any case be seen as a minor departure from standard inclining seashore, however it is as of now progressively refined. It was planned by Marcou in 1954. The absorber comprises of a slim aluminium plate that on its right side is resting in its corners on an edge and that on its left side can turn around a pivot indicated with O in Figure. The plate is brought and brought down up in an occasional manner under the episode wave assault. Each incident wave pushes the plate against its backings, however during running over the plate the wave breaks and rather than the past wave absorbers the water from the crushing wave isn't going spirit to the flume however this water and the vitality which it has is cleared as it streams over the highest point of the plate, winding up in the compartment at the rear of the plate. When the episode wave is passed, the plate springs back a piece and comes free from its backings.

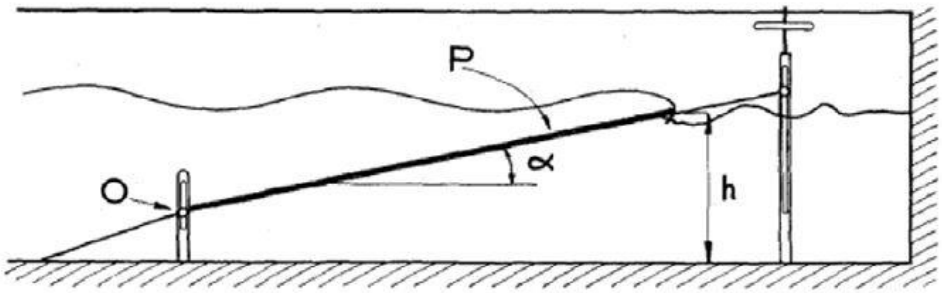

Figure 31: Marcou wave absorber

4.8 Perforated Slope:

This wave absorber is much the same as the past two attempting to keep the water from the breaking waves from streaming promptly once more into the flume. This is finished by utilizing a slope, which comprises of a punctured wooden plate. All things considered the water from the breaking waves moves through the plate to the rear of it where it is guided by ten short plates to the base of the flume. Here, the water is all the calmer and it can stream once again into the flume making less aggravations the occurrence waves. Reflection coefficients for this wave absorber are found to extend somewhere in the range of 0.05 and 0.2.

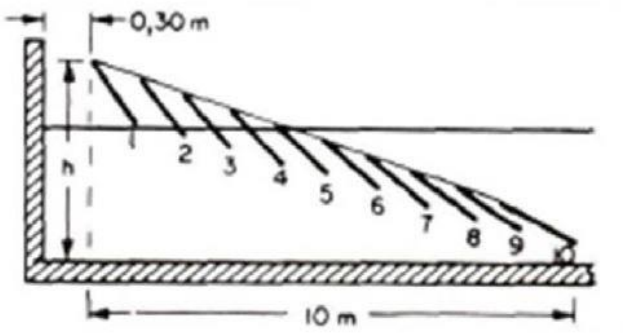

Figure 32: Perforated slop wave absorber

4.9 Parabolic Slope:

This wave absorber doesn't have a straight slope any longer. The slope of the absorber has, be that as it may, an illustrative shape. This has a similar favourable position as the wave absorbers talked about before, by picking an explanatory shape for the cross-segment of the

seashore, the littlest slope is present where the water has the most vitality, for example in the perimeter of the still water level. As a result, the wave vitality is dispersed all the more proficiently. Various materials are feasible for this wave absorber, going from rock over transversal bars to wire screens.

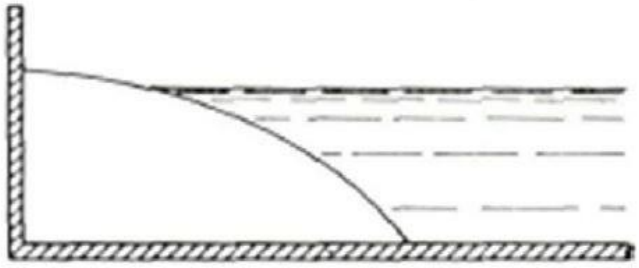

Figure 33: Parabolic slop wave absorber

4.10 Parabolic Slope without Bottom:

This wave absorber is a variation on the past one. Rather than the standard illustrative slope, this wave absorber doesn't arrive at the base. This spares material and lessens the length of the absorber. The expansion of the reflection coefficient is little because of the way that at higher profundities the wave vitality is little. The majority of the vitality is arranged at lower profundities and here the parabola is present to scatter this vitality. Anyway, the utilization of this wave absorber is again addressed in shallow water where the wave vitality is spread all the more equitably over the depth.

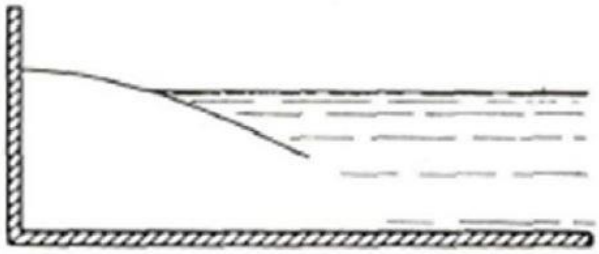

Figure 34: Bottomless parabolic slop wave absorber

4.11 Combination of Straight and Parabolic Slope:

This wave absorber is a blend of both a straight and parabolic slope. A straight slope is set at the base and three diverse explanatory slopes are put over. The absorber is made out of a wire screen in mix with a transversal bars, sand, rock and stones. No data on the reflection

coefficient can be found. Be that as it may, the reflection coefficient of this wave absorber will obviously be subject to the pre-owned estimation of the straight slope.

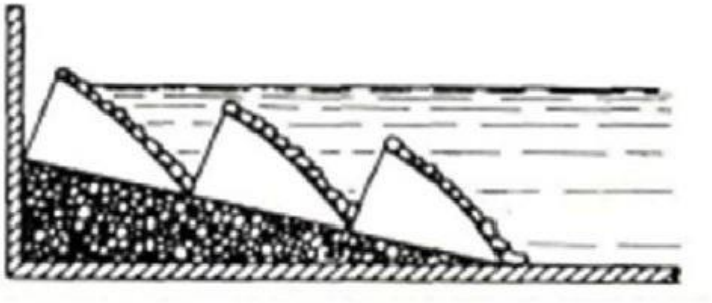

Figure 35: Combination of straight and parabolic slop

4.12 Vertical Mesh Wave Absorber:

In this arrangement vertical punctured plates with a specific dividing in between them are set toward the finish of the wave flume to work as a wave absorber. As the water needs to course through the openings of the back to back punctured plates the wave energy is dispersed, and the abundancy of the reflected wave turns out to be little which brings about a little reflection coefficient. Obviously, this reflection coefficient will diminish with expanding sum of vertical plates, however utilizing a high measure of plates would assume a ton of position in a wave flume and wouldn't be conservative. Additionally, it is naturally evident that the more vertical plates there are as of now introduced the littler the commitment of an additional vertical plate to the abatement of the reflection coefficient will be. The inquiry presently raises from which measure of plates onwards the impact of including an extra plate can be disregarded as for the additional room and cost it makes. Other than this it is likewise significant to know the perfect dividing between the vertical plates so as to limit the reflection coefficient.

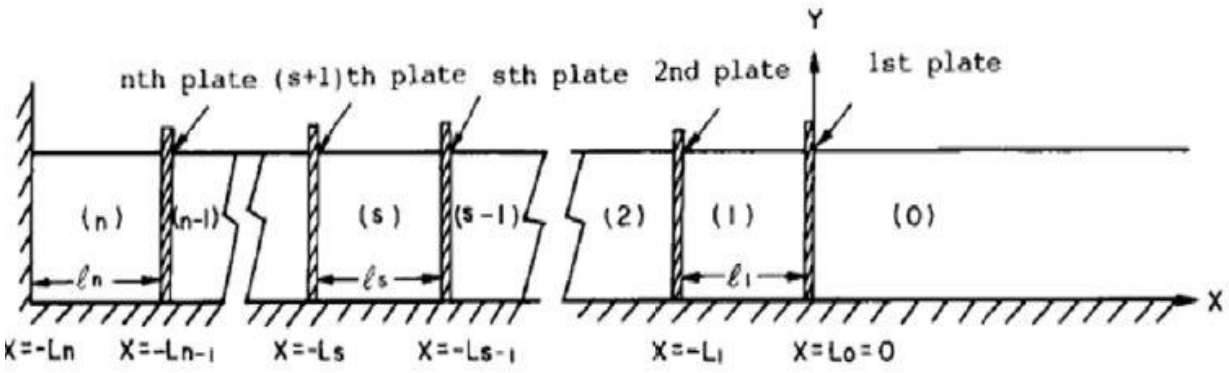

Figure 36: Vertical mesh wave absorber

4.13 Mesh Screens:

This wave absorber utilizes a progression of work screens to scatter the wave vitality as is portrayed in Figure. One could consider this to be absorber as a minor departure from the vertical work with the lattices set exceptionally near one another. The reflection coefficient shifts a great deal. Qualities among 0.05 and 0.92 are conceivable. This wave absorber is very porous, as the porousness approaches 92%.

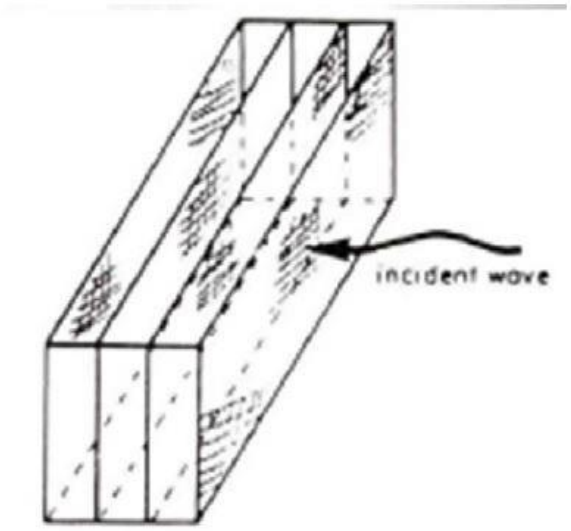

Figure 37: Mesh screen

CHAPTER 5: EXPERIMENTAL SETUP

Experiments were conducted in a wave flume having transparent test section of 2000 × 400 × 500 mm (L × W × H). Waves were generated using flap type wave maker fixed at one end of the tunnel.

Figure 38: Experimental setup of wave generator with adjustable flapper amplitude

Vertical mesh type wave absorber was fixed at the other end to damp out the incoming waves and to reduce the wave reflection. Schematic diagrams of the complete experimental setup are described in figure 39 and 40.

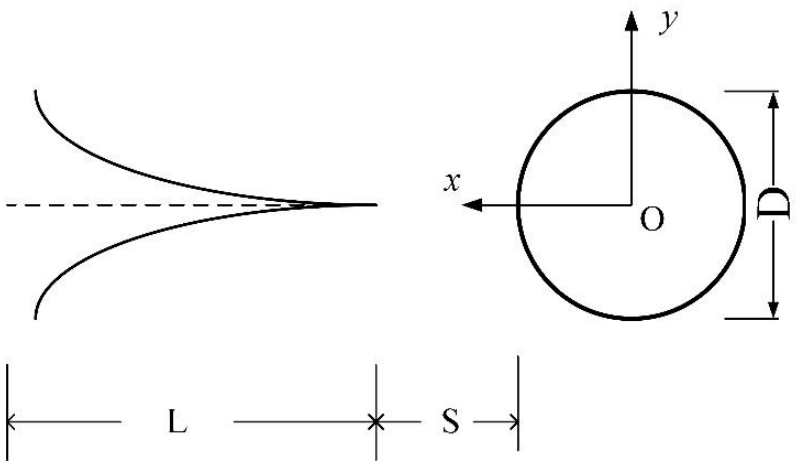

Figure 39: Schematic Diagram

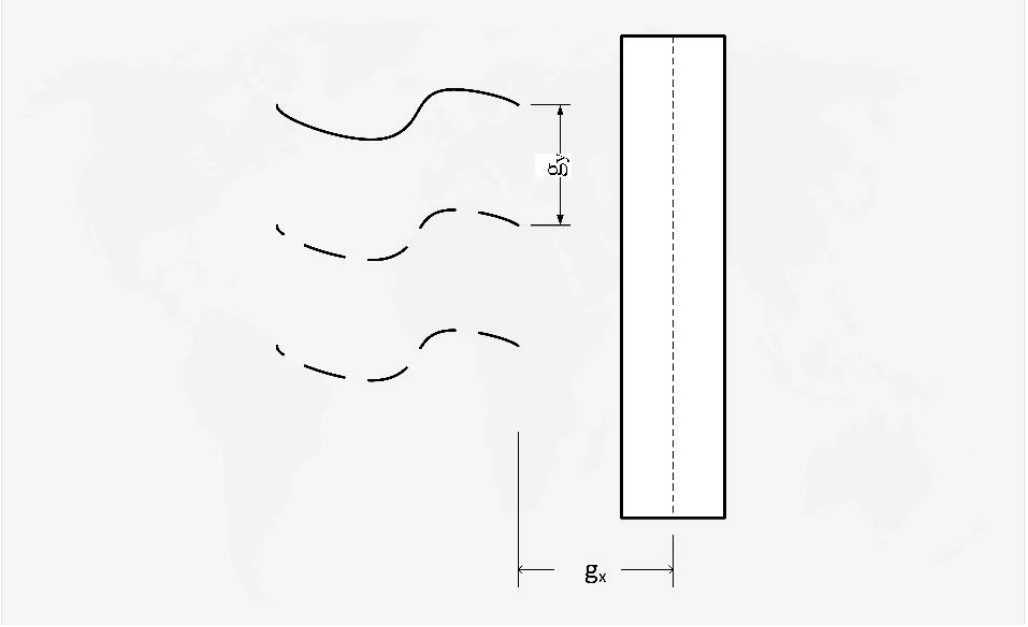

Figure 40: Schematic representation of piezoelectric eel and cylinder as a function of G_y

A flexible PVDF eel DT2-052K with lead attachments by Measurement Specialties, Inc. was used for energy harvesting.

Table 1: Piezoelectric Eel Physical Properties

Material	Young's Modulus	Poisson's ratio	Density	Height (Sheet)	Length (Sheet)	Diameter of Cylinder
PVDF	$E-1.38e^{9}Nm^{2}$	$\nu-0.46$	$\rho_S=0.96e^{3}kg$	$H-16mm$	$L-62mm$	$D-25mm$

Note: All units are in SI

Parameter	Units	Value
Capacitance @ 1KHz	pF/m	600
Acoustic Impedance	MRayl	4.0
Relative Permittivity	@1KHz	9
tan äe	@1KHz pC/N	0.017
Hydrostatic Piezo Coefficient	Vm/N	15
Longitudinal Piezo Coefficient	Vm/N	250×10^{-3}
Hydrostatic Piezo Coefficient		150×10^{-3}
Electromechanical Coupling	%	20
Energy Output	mJ/Strain (%)	10
Voltage Output	kV/Strain (%)	5

The dimensions of the piezoelectric eel are 62 mm length (L) and 12 mm width (W). Solid frame structure was used to hold the piezoelectric eel with fixed leading edge and free trailing edge capable of adjusting position behind the fixed vertical cylinder. Circular cylinder with 25 mm diameter was used as a bluff body and eel was mounted in the wake of this cylindrical bluff body.

Table 2: Piezoelectric Eel Mechanical Properties

Symbol	Parameter		PVDF	Units
t	Thickness		52	µm (micron, 10-6)
d31 d33	Piezo Strain Constant		23 -33	10-12
g31 g33	Piezo Stress constant		216 -330	10-3
k31 kt	Electromechanical Coupling Factor		12% 14%	
Y	Young's Modulus		2-4	109 N/m2
V0	Speed of Sound	stretch: thickness:	1.5 2.2	103 m/s
p	Pyroelectric Coefficient		30	10-6 C/m2 °K
å	Permittivity		106-113	10-12 F/m
å/å 0	Relative Permittivity		12-13	
ρ_m	Mass Density		1.78	103kg/m
ρ_e	Volume Resistivity		>1013	Ohm meters
$R_\square$ $R_\square$	Surface Metallization Resistivity		<3.0 0.1	Ohms/square for NiCu Ohms/square for Ag Ink
tan äe	Loss Tangent		0.02	@ 1KHz
	Yield Strength		45-55	106 N/m2 (stretch axis)
	Temperature Range		-40 to 80...100	∘ C
	Water Absorption		<0.02	% H2O
	Maximum Operating Voltage		750 (30)	V/mil (V/µm), DC, @ 25°C
	Breakdown Voltage		2000 (80)	V/mil (V/µm), DC, @ 25°C

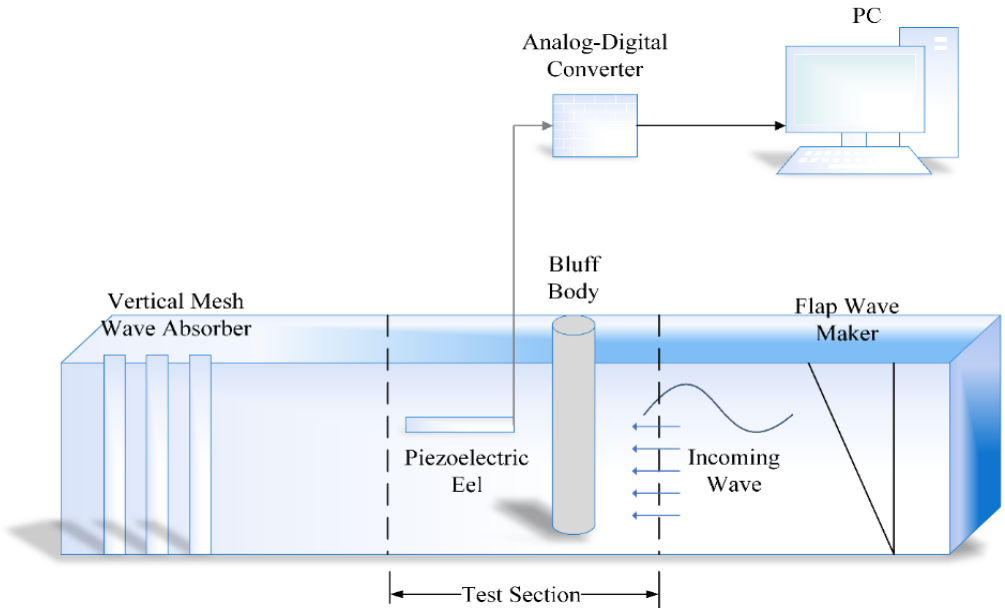

Figure 41: Schematic representation of complete experimental setup

Waves with different characteristics/parameters were generated as described in table 1. For all wave conditions, the streamwise gap G_x, from cylinder was varied from S/D= 0.75 to 1.75 and spanwise gap from G_y = H/2 to 3H/2 as represented by top view and side view in figure 40. A DC motor was used to operate wave maker at different RPM/speed with the help of DC power supply GW INSTEK GPS-2303.

Figure 42: Experimental setup

Undulating behaviour of eel was monitored by using high speed camera "Sony Cyber-shot DSC-RX100 IV" mounted under the transparent bed of test section and recorded the videos at the rate of 50 fps due to viscous fluid. Test section was illuminated with LED lights, Data acquisition was done by using DAQ card (National Instruments, USB-6009) with LabView® software and sample rate was set to 50 Hz. MATLAB™ image processing technique was used to process the recorded videos and flapping envelop is shown as superposition of the captured images.

Table 3: Wave parameters

Wave Period (sec)	Wavelength (mm)	Wave Height (mm)	Steepness Ratio H/ λ
0.71	790	60	0.075
0.65	660	65	0.098
0.6	560	70	0.125
0.57	508	75	0.147

CHAPTER 6: RESULTS AND DISCUSSION

6.1 Case 1:

Piezoelectric eel spanwise gap was fixed at $G_{y=}$ H/2 (near the water surface) and flag dynamics were investigated by changing stream-wise distance G_x at different wave conditions. Energy of the wave decayed as we gradually increased the depth. Water particles become unaffected as depth approaches to λ/2 [15]. At fixed G_y, cylinder vortices and hence piezoelectric eel deformation majorly depends upon wavelength λ, wave height H, and streamwise distance from the bluff body G_x, as represented in Figure 43. Maximum and minimum peak to peak flapping displacement is represented by a superimposed image of flag at different streamwise distance G_x and wave conditions in Figure 43 with their corresponding time scale history of flapping for 10 seconds as in shown Figure 43 a & b. At longer wavelength for range of gap, corresponding wave height is small, resulting in a small-scale non-phase-locked vortex formation which undergoes small deformation in the piezo eel. At shorter wavelength for a range of streamwise gap, wave height increases which led to formation of strong vorticity concentration and thus increase strain energy in piezo eel. This behaviour is due to the circular orbital motion of water particles largely effected by wave height as orbital diameter is the height of the wave [19].

Figure 43 shows the output voltage, peak to peak amplitude and flapping frequency response at fixed span-wise gap G_y while altering wavelength, wave height and streamwise gap. A general trend of increasing voltage for decreasing wavelength can be observed for all stream-wise distance G_x. Flapping frequency and peak to peak amplitude shows reverse behaviour for increasing gap which can be supported by cylinder vortices. Vortex formed adjacent to the surface of cylinder which grows to specific distance and finally dissipate their energy while gap increases at fixed depth [23]. Point 1 in Figure 433(a) represents the maximum output voltages (V_{rms} = 1.43v) at λ= 508 mm and G_x = 1.25 followed by a large flapping amplitude A/L= 0.48 and flapping frequency FF= 0.06 as shown by flag envelop in Figure 44(b) and its peak amplitude time scale response in Figure 44(a). Higher flapping amplitude and frequency causes higher strain rate resulting in high voltage generation. Similarly point 2 in Figure 433(a) shows the minimum output voltages (V_{rms} = 0.56v) generated at λ=790 mm and G_x=1.75 caused by low peak to peak amplitude A/L= 0.11 and flapping frequency FF= 0.05 represented by flapping envelop in Figure 44(d) and corresponding time scale amplitude in Figure 44(c).

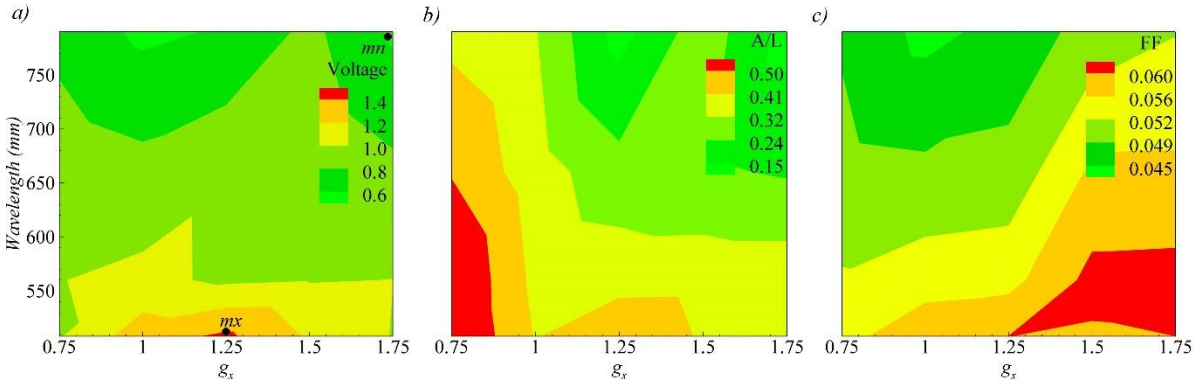

Figure 43 : Contour plot of a) Root mean square voltage b) Flapping amplitude A/L c) Flapping frequency, as a function of wavelength and streamwise gap (S/D) for G_y= H/2.

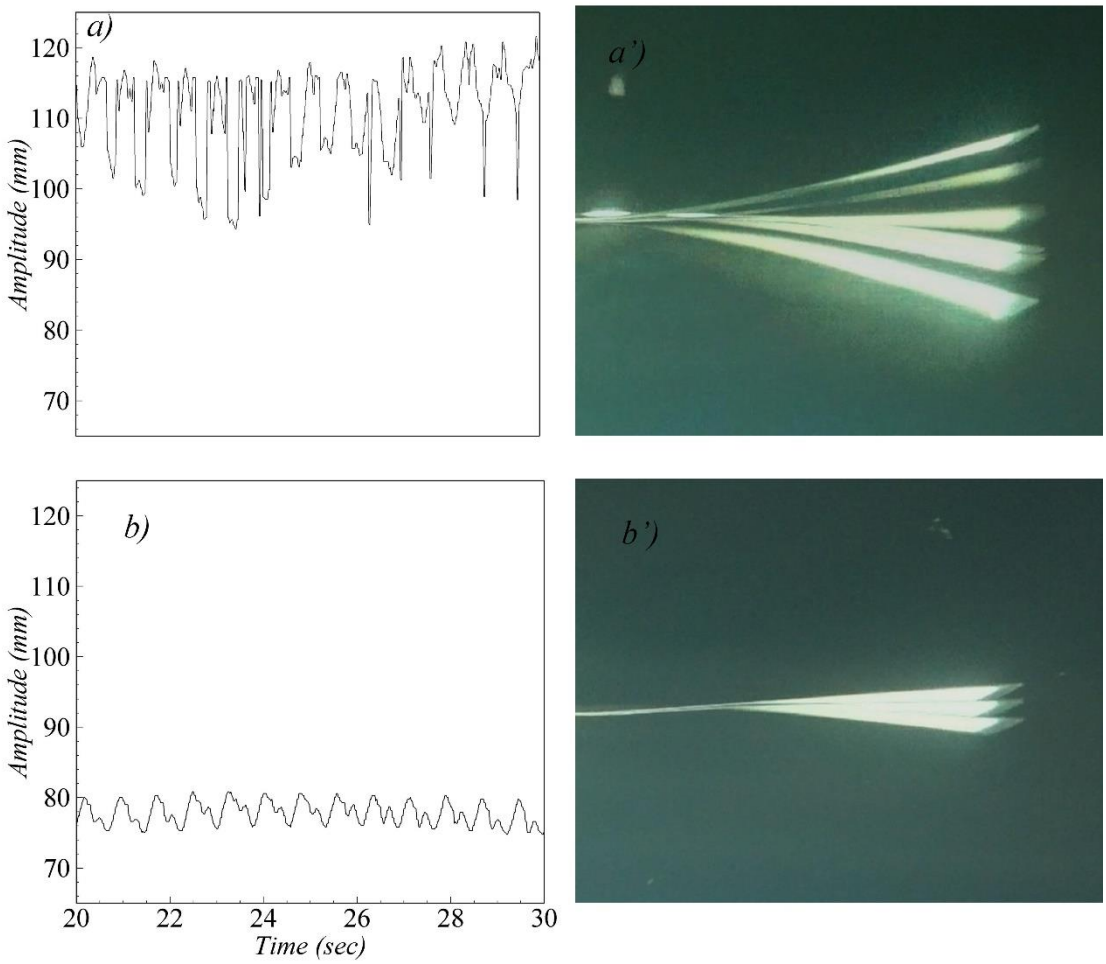

Figure 44: a) Amplitude behavior and b) corresponding superimposed image of flag at S/D=1.25 and L=508mm c) & d) represent peak to peak amplitude A/L and superimposed envelop respectively at S/D=1.75 and λ =790mm.

6.2 Case 2:

Piezoelectric eel span-wise gap increased from G_y = H/2 to H and flag deformation was studied under same wave conditions and streamwise distance G_x as used for the case-1. Increase in the submergence depth decreases diameter of particle orbital motion [21], which results in low peak to peak amplitude A/L as compared with case 1. Figure. 45 shows the surface plot of voltages V_{rms}, flapping amplitude and frequency. Furthermore, in Figure. 45(a) point 1 indicates maximum root mean square voltage V_{rms}=1.28v at λ=508 mm and G_x=1.25 caused by flapping amplitude A/L=0.4 and flapping frequency FF=0.06. Figure. 46(a) and Figure. (b) show their corresponding peak to peak amplitude response and flag envelop respectively.

At shorter wavelength and close to the cylinder G_x < 1.5, cylinder wakes dominate which results in large flapping amplitude, but maximum peak to peak amplitude is less than the previous case due to decrease in particle orbital diameter at greater depth. Along the span of cylinder, patterns of velocity and vorticity decreases due to decrease in local wavelength beneath the free surface [29].

Whereas point 2 in Figure. 45(a) indicates the minimum root mean square voltage (V_{rms}=0.6v) at λ=790 mm and G_x=0.75 due to minimum peak to peak amplitude A/L=0.14 and flapping frequency FF=0.04 as represented by envelop of superimposed images in Figure. 46(d) and amplitude as a function of time in Figure. 46(c). Longer wavelength with smaller wave amplitude produced less strain in the flag. As it can be observed in surface plot, longer the wavelength the lesser the deformation produced in the piezoelectric eel. As a result, good voltage region can be observed till wavelength λ=660mm for all range of streamwise distance G_x but further increasing the wavelength causes drop in voltage region up to λ=790mm.

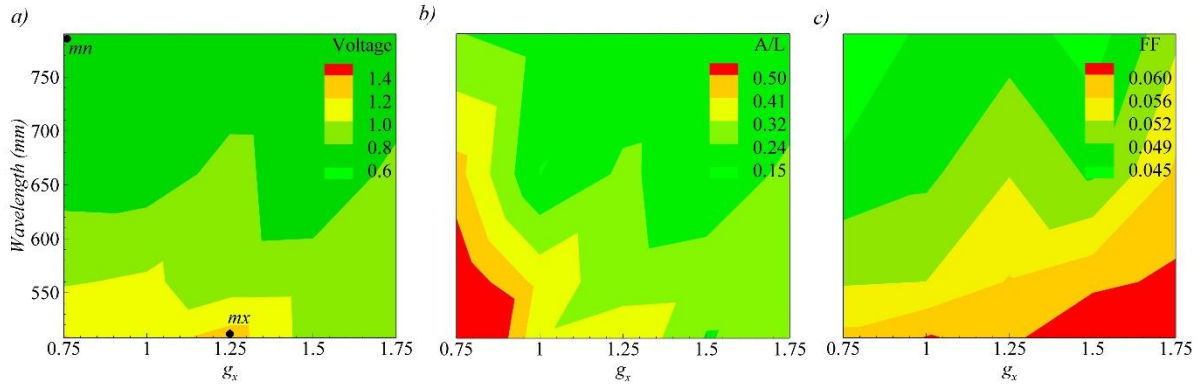

Figure 45 : a) Root mean square voltage b) Peak to peak amplitude c) Flapping frequency, as a function of wavelength and streamwise gap (S/D) for device depth location G_y=H.

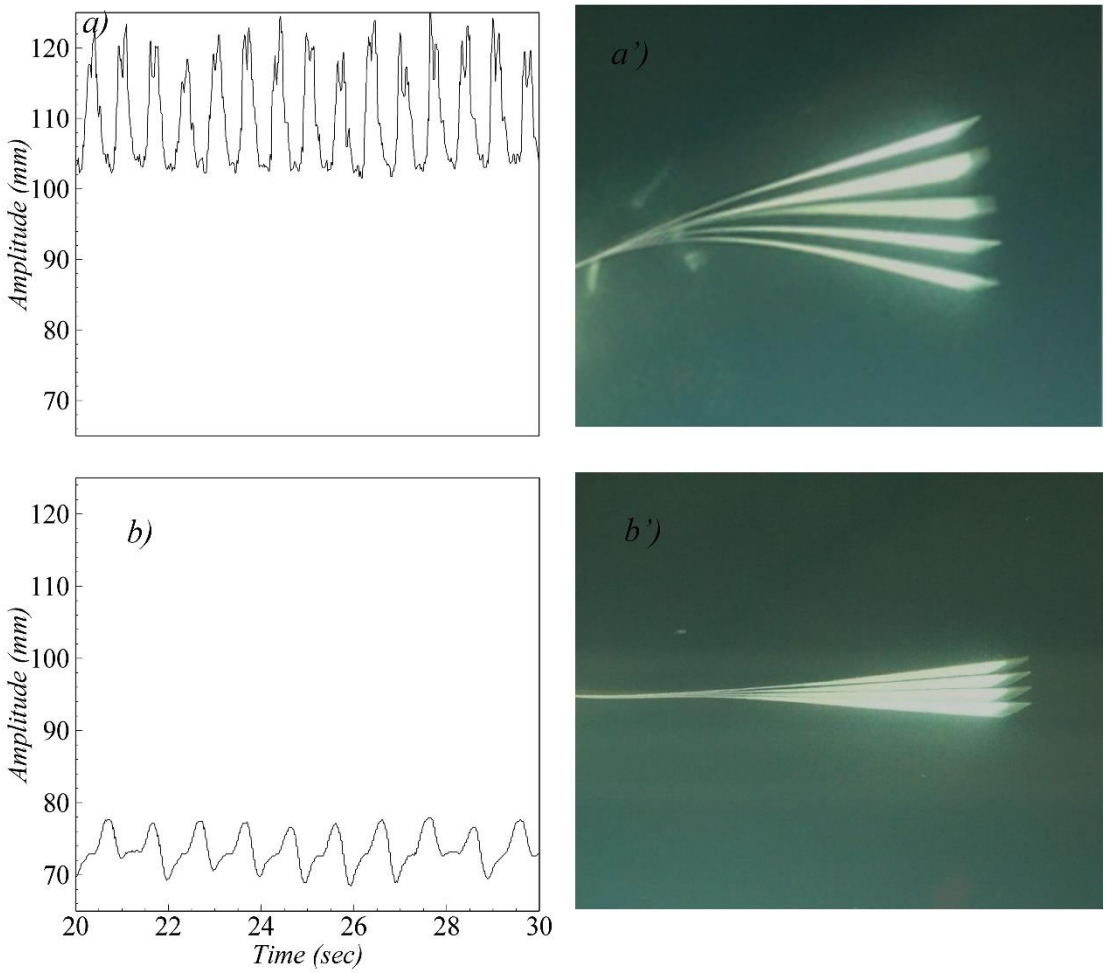

Figure 46 : a) Flapping amplitude behaviour b) corresponding superimposed envelop of flag at S/D=1.25 and λ= 508mm. c) & d) represent peak to peak amplitude (A/L) and superimposed envelop respectively at S/D= 0.75 and λ= 790mm.

6.3 Case 3:

Piezoelectric eel span-wise gap was further increased to maximum G_y of 3H/2 and flag flapping dynamics was observed under the mentioned wave conditions and streamwise gap. Case 3 is different from previous both cases due to fragile wave effect in deeper level. From Figure. 47(a) it can be observed that the maximum voltage generated caused by flag deformation as represented in Figure. 48(b) and (c) is less than the previous cases due to small wave amplitude. At larger depth, magnitude of the particle orbits decreases and orbital circular motion is converted into horseshoe-shaped induced by return flow [26]. Point 1 in Figure. 47(a) shows the maximum output voltage V_{rms}=0.98v at wavelength λ=508mm and S/D=1.25 caused by their corresponding peak to peak amplitude A/L=0.27 and flapping frequency FF=0.06.

Figure. 48(a) and Figure. 48(b) illustrate the amplitude response and flag flapping envelop at point 1 respectively.

Contrary to case 1 & 2, voltage region is negligible despite at shorter wavelength for all range of streamwise gaps. But at G_x=1.25, voltage region is considerable for all wavelengths. In larger depth beneath the free surface, optimal energy output reached and surpassed, due to relationship between wave velocity, fluid forcing and fluid damping [48].

Figure. 48 (c) represent the flapping frequency which became the focus of interest. High flapping region can be observed at shorter wavelength at all streamwise gaps unlike to the previous cases. This is due to the fact that, water particle orbital diameter decreases progressively with depth, as a result smaller orbit caused large flapping with low peak to peak amplitude.

Point 2 in Figure. 47(a) indicate the minimum voltage generation V_{rms}=0.5v at wavelength λ=790 mm and G_x=0.75, illustrated by flapping envelop in Figure. 48(d) and peak to peak amplitude in Figure. 48(c). At higher submergence depth, low amplitude wave result in low peak amplitude A/L=0.08 and minimum flapping frequency FF=0.05.

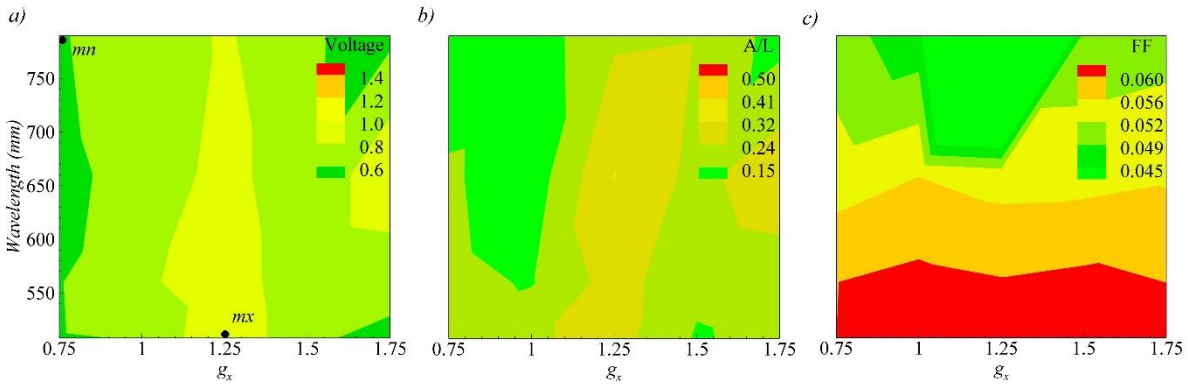

Figure 47 : a) Root mean square voltage b) Peak to peak amplitude (A/L) c) Flapping frequency, as a function of wavelength and streamwise gap (S/D) for device depth= 3H/2.

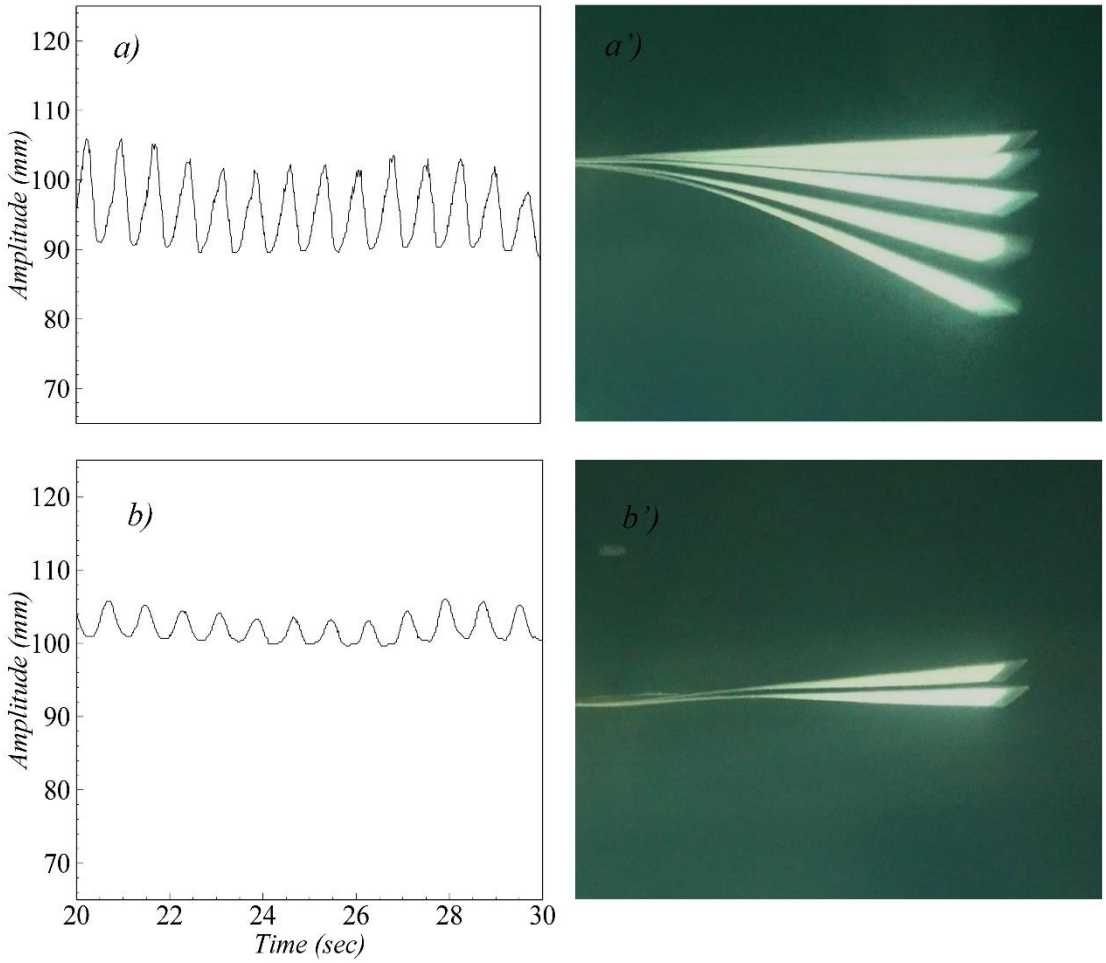

Figure 48 : a) Flapping amplitude behavior b) corresponding superimposed envelop of flag at S/D=1.25 and λ= 508mm. c) & d) represent peak to peak amplitude (A/L) and superimposed envelop respectively at S/D= 0.75 and λ= 790 mm.

6.4 All Cases Comparison:

Piezoelectric flag dynamics was affected by changing the span-wise gap below the free surface G_y=H/2 to 3H/2 and stream-wise distance from fixed cylinder G_x=0.75 to 1.75 for range of wavelength λ=508mm to 790mm. Maximum voltage (V_{rms}= 1.43v) was achieved in case 1 at G_x=1.25 and λ= 508mm where the flag is near to the free surface. As concentration of velocity and vorticity in the wake of circular cylinder highly dependent on local wavelength and wave amplitude [11]. Furthermore, wave particle orbit diameter is large near the surface and decrease gradually with depth [7].

Similarly, minimum voltage (V_{rms}= 0.5v) was obtained at deeper depth (3H/2) due to decrease in orbital diameter and small wave affect. Vortex formation is closely allied with depth along the span of vertical cylinder [6].

Figure. 50 provides the comparison of voltage V_{rms}, peak amplitude (A/L) and flapping frequency (FF) for all 3 cases. Voltage region for case 1 and 2 is similar in both cases following with similar flapping amplitude region and frequency region. At shorter wavelength of λ=508mm, high voltage was observed for all G_x and maximum at G_x=1.25. In contrast, low voltage region was observed in case 3 for all G_x except at G_x=1.25 where measurable voltage region was obtained for all wavelengths.

Figure. 49(a) provides the comparison of output voltage as a function of wavelength for all span-wise gap G_y at fixed streamwise distance of G_x=1.25. Similarly, comparison of output voltage at streamwise distance G_x=0.75 is shown in Figure. 49(b).

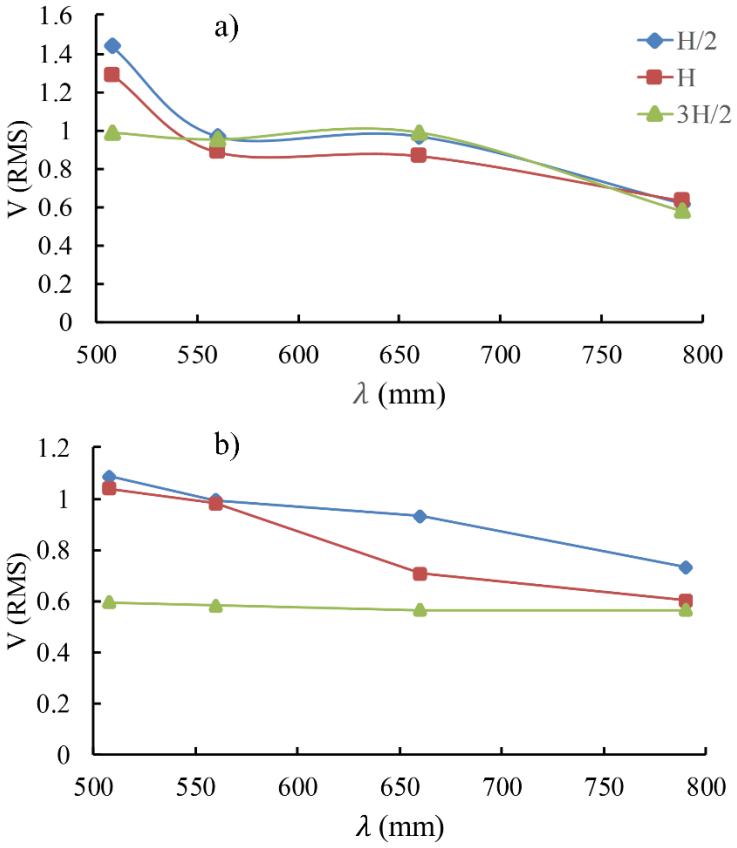

Figure 49: Output voltage as a function of wavelength for all submergence depth at a) S/D=1.25 b) S/D= 0.75

A general trend of high voltage region was observed between streamwise distance G_x= 1~1.5 and wavelength $\lambda \leq 660$mm for all spanwise gap. While at longer wavelength $\lambda > 660$mm, very low voltage region was observed for all streamwise and spanwise distance as shown by figure 48.

By observing Figure 50, it can be noted that at G_x=1.75 maximum horizontal distance from cylinder, a good voltage region was obtained at shorter wavelength λ=508mm to 660mm for all three cases. As close to the cylinder flag flapped in the wakes of cylinder, on moving away from cylinder to G_x=1.75 wakes dissipated their energy and flag flapped due to orbital circular motion of water particles. Apart from this, conflicting behaviour of flapping frequency for case 3 is due to small orbital diameter of water particle at greater depth.

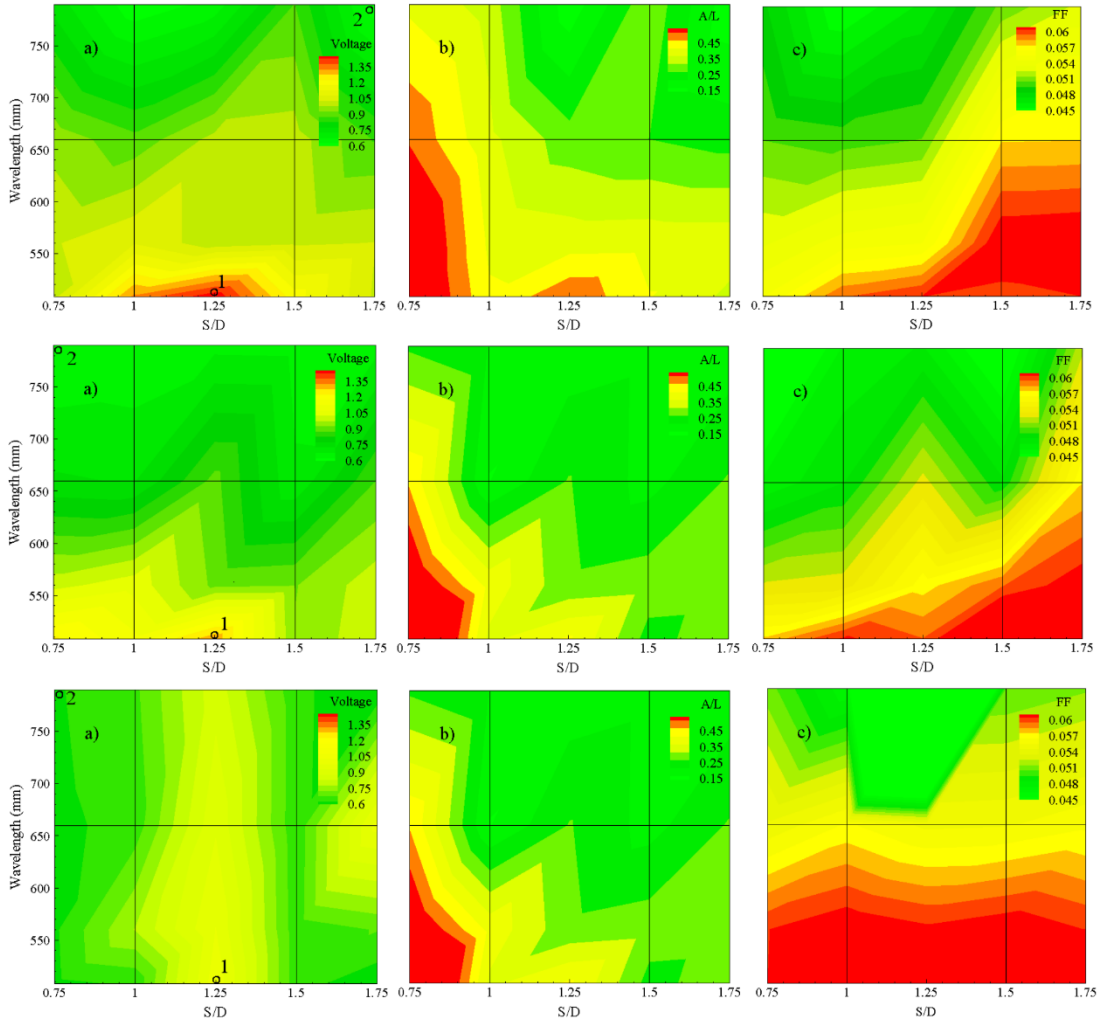

Figure 50 : Contour plots of V_{rms}, peak to peak amplitude (A/L) and flapping frequency for all three cases.

6.5 Conclusion:

Energy harvesting was studied by flapping of flexible piezoelectric eel caused by vortex-induced vibration (VIV) behind fixed vertical circular cylinder under different wave conditions. Piezoelectric flag behaviour was captured using high speed camera and voltage was calculated for range of streamwise gap and spanwise distance along the cylinder and are represented by contour plots as a function of wavelength. Three cases were performed for different depth location for all range of wavelength and streamwise gap. For all 3 cases output voltage and flag behaviour was studied and represented. It was observed that wake was highly dependent on wave height and local wavelength beneath the free surface. Near the free surface voltage obtained was maximum caused by high peak to peak amplitude and flapping frequency due to larger particle orbital diameter and strong vortex interaction. It was observed that for all cases good result was obtained at streamwise distance G_x=1.25 and at shorter wavelength. Similarly, minimum voltage was calculated at longer wavelength and at greater depth. As submergence depth increases, output voltage decreases and minimum voltage was calculated at maximum submergence depth. At greater depth, orbital diameter decreases and concentration of vorticity reduces due to weak wave effect. By using the array of piezoelectric eel, energy harvesting system studied in this paper can be used to power low power electronics in the ocean buoys in deep water waves.

REFERENCES

[1] E. Uddin, W.-X. Huang, and H. J. Sung, "Interaction modes of multiple flexible flags in a uniform flow," *Journal of Fluid Mechanics,* vol. 729, pp. 563-583, 2013.

[2] S. Alben, "Simulating the dynamics of flexible bodies and vortex sheets," *Journal of Computational Physics,* vol. 228, no. 7, pp. 2587-2603, 2009.

[3] S. Alben and M. J. Shelley, "Flapping states of a flag in an inviscid fluid: bistability and the transition to chaos," *Physical review letters,* vol. 100, no. 7, p. 074301, 2008.

[4] W.-X. Huang and H. J. Sung, "An immersed boundary method for fluid–flexible structure interaction," *Computer Methods in Applied Mechanics and Engineering,* vol. 198, no. 33-36, pp. 2650-2661, 2009.

[5] J. Zhang, S. Childress, A. Libchaber, and M. Shelley, "Flexible filaments in a flowing soap film as a model for one-dimensional flags in a two-dimensional wind," *Nature,* vol. 408, no. 6814, p. 835, 2000.

[6] L. Tang, M. P. Païdoussis, and J. Jiang, "Cantilevered flexible plates in axial flow: energy transfer and the concept of flutter-mill," *Journal of Sound and Vibration,* vol. 326, no. 1-2, pp. 263-276, 2009.

[7] S. J. Lighthill, *Mathematical biofluiddynamics*. SIAM, 1975.

[8] D. Ishihara, T. Horie, and M. Denda, "A two-dimensional computational study on the fluid–structure interaction cause of wing pitch changes in dipteran flapping flight," *Journal of Experimental Biology,* vol. 212, no. 1, pp. 1-10, 2009.

[9] K. Shoele and Q. Zhu, "Performance of synchronized fins in biomimetic propulsion," *Bioinspiration & biomimetics,* vol. 10, no. 2, p. 026008, 2015.

[10] D. Tang, H. Yamamoto, and E. Dowell, "Flutter and limit cycle oscillations of two-dimensional panels in three-dimensional axial flow," *Journal of Fluids and Structures,* vol. 17, no. 2, pp. 225-242, 2003.

[11] J. Pirnar, L. Dolenc-Grošelj, I. Fajdiga, and I. Žun, "Computational fluid-structure interaction simulation of airflow in the human upper airway," *Journal of biomechanics,* vol. 48, no. 13, pp. 3685-3691, 2015.

[12] M. K. Nandwana, A. Ziaei, and J. H. Hansen, "Robust unsupervised detection of human screams in noisy acoustic environments," in *2015 IEEE International Conference on Acoustics, Speech and Signal Processing (ICASSP)*, 2015: IEEE, pp. 161-165.

[13] K. Shoele and R. Mittal, "Energy harvesting by flow-induced flutter in a simple model of an inverted piezoelectric flag," *Journal of Fluid Mechanics,* vol. 790, pp. 582-606, 2016.

[14] O. Doaré and S. Michelin, "Piezoelectric coupling in energy-harvesting fluttering flexible plates: linear stability analysis and conversion efficiency," *Journal of Fluids and Structures,* vol. 27, no. 8, pp. 1357-1375, 2011.

[15] S. Michelin and O. Doaré, "Energy harvesting efficiency of piezoelectric flags in axial flows," *Journal of Fluid Mechanics,* vol. 714, pp. 489-504, 2013.

[16] C. Guo, "Analysis of hydroelastic instabilities of rectangular parallel-plate assemblies," *Journal of Pressure Vessel Technology,* vol. 122, no. 4, pp. 502-508, 2000.

[17] A. Giacomello and M. Porfiri, "Underwater energy harvesting from a heavy flag hosting ionic polymer metal composites," *Journal of Applied Physics,* vol. 109, no. 8, p. 084903, 2011.

[18] J. Dunnmon, S. Stanton, B. Mann, and E. Dowell, "Power extraction from aeroelastic limit cycle oscillations," *Journal of Fluids and Structures,* vol. 27, no. 8, pp. 1182-1198, 2011.

[19] M. P. Paidoussis, *Fluid-structure interactions: slender structures and axial flow*. Academic press, 1998.

[20] M. J. Shelley and J. Zhang, "Flapping and bending bodies interacting with fluid flows," *Annual Review of Fluid Mechanics,* vol. 43, pp. 449-465, 2011.

[21] Z. Peng and Q. Zhu, "Energy harvesting through flow-induced oscillations of a foil," *Physics of fluids,* vol. 21, no. 12, p. 123602, 2009.

[22] S. Michelin, S. G. L. Smith, and B. J. Glover, "Vortex shedding model of a flapping flag," *Journal of Fluid Mechanics,* vol. 617, pp. 1-10, 2008.

[23] D. T. Akcabay and Y. L. Young, "Hydroelastic response and energy harvesting potential of flexible piezoelectric beams in viscous flow," *Physics of Fluids,* vol. 24, no. 5, p. 054106, 2012.

[24] J. Allen and A. Smits, "Energy harvesting eel," *Journal of fluids and structures,* vol. 15, no. 3-4, pp. 629-640, 2001.

[25] K. Singh, S. Michelin, and E. de Langre, "Energy harvesting from axial fluid-elastic instabilities of a cylinder," *Journal of Fluids and Structures,* vol. 30, pp. 159-172, 2012.

[26] K. Singh, S. Michelin, and E. De Langre, "The effect of non-uniform damping on flutter in axial flow and energy-harvesting strategies," *Proceedings of the Royal Society A:*

Mathematical, Physical and Engineering Sciences, vol. 468, no. 2147, pp. 3620-3635, 2012.

[27] E. Virot, "Flottement de drapeau: dynamique et couplage," 2015.

[28] B. S. Connell and D. K. Yue, "Flapping dynamics of a flag in a uniform stream," *Journal of fluid mechanics*, vol. 581, pp. 33-67, 2007.

[29] H. S. Kim, J.-H. Kim, and J. Kim, "A review of piezoelectric energy harvesting based on vibration," *International journal of precision engineering and manufacturing*, vol. 12, no. 6, pp. 1129-1141, 2011.

[30] S. R. Anton and H. A. Sodano, "A review of power harvesting using piezoelectric materials (2003–2006)," *Smart materials and Structures*, vol. 16, no. 3, p. R1, 2007.

[31] H. D. Akaydin, N. Elvin, and Y. Andreopoulos, "Energy harvesting from highly unsteady fluid flows using piezoelectric materials," *Journal of Intelligent Material Systems and Structures*, vol. 21, no. 13, pp. 1263-1278, 2010.

[32] S. Taneda, "Waving motions of flags," *Journal of the Physical Society of Japan*, vol. 24, no. 2, pp. 392-401, 1968.

[33] T. Y.-T. Wu, "Swimming of a waving plate," *Journal of Fluid Mechanics*, vol. 10, no. 3, pp. 321-344, 1961.

[34] A. Kornecki, E. Dowell, and J. O'brien, "On the aeroelastic instability of two-dimensional panels in uniform incompressible flow," *Journal of Sound and Vibration*, vol. 47, no. 2, pp. 163-178, 1976.

[35] L. Huang, "Flutter of cantilevered plates in axial flow," *Journal of Fluids and Structures*, vol. 9, no. 2, pp. 127-147, 1995.

[36] C. Eloy, C. Souilliez, and L. Schouveiler, "Flutter of a rectangular plate," *Journal of Fluids and Structures*, vol. 23, no. 6, pp. 904-919, 2007.

[37] Y. Watanabe, S. Suzuki, M. Sugihara, and Y. Sueoka, "An experimental study of paper flutter," *Journal of fluids and Structures*, vol. 16, no. 4, pp. 529-542, 2002.

[38] C. Eloy, N. Kofman, and L. Schouveiler, "The origin of hysteresis in the flag instability," *Journal of Fluid Mechanics*, vol. 691, pp. 583-593, 2012.

[39] E. Virot, X. Amandolese, and P. Hémon, "Fluttering flags: an experimental study of fluid forces," *Journal of fluids and structures*, vol. 43, pp. 385-401, 2013.

[40] S. C. Gibbs, I. Wang, and E. Dowell, "Theory and experiment for flutter of a rectangular plate with a fixed leading edge in three-dimensional axial flow," *Journal of Fluids and Structures*, vol. 34, pp. 68-83, 2012.

[41] L. Zhu and C. S. Peskin, "Simulation of a flapping flexible filament in a flowing soap film by the immersed boundary method," *Journal of Computational Physics,* vol. 179, no. 2, pp. 452-468, 2002.

[42] J. Curie and P. Curie, "Sur l'électricité polaire dans les cristaux hémièdres à faces inclinées," *CR Acad Sci Gen,* vol. 91, pp. 383-6, 1880.

[43] G. Lippmann, "Principe de la conservation de l'électricité, ou second principe de la théorie des phénomènes électriques," *Journal de Physique Théorique et Appliquée,* vol. 10, no. 1, pp. 381-394, 1881.

[44] J. Curie and P. Curie, "Contractions et dilatations produites par des tensions électriques dans les cristaux hémièdres à faces inclinées," *Compt. Rend,* vol. 93, pp. 1137-1140, 1881.

[45] K. S. Ramadan, D. Sameoto, and S. Evoy, "A review of piezoelectric polymers as functional materials for electromechanical transducers," *Smart Materials and Structures,* vol. 23, no. 3, p. 033001, 2014.

[46] P. Bisegna, G. Caruso, and F. Maceri, "Optimized electric networks for vibration damping of piezoactuated beams," *Journal of Sound and Vibration,* vol. 289, no. 4-5, pp. 908-937, 2006.

[47] O. Thomas, J. F. Deü, and J. Ducarne, "Vibrations of an elastic structure with shunted piezoelectric patches: efficient finite element formulation and electromechanical coupling coefficients," *International journal for numerical methods in engineering,* vol. 80, no. 2, pp. 235-268, 2009.

[48] J. Ducarne, O. Thomas, and J.-F. Deü, "Placement and dimension optimization of shunted piezoelectric patches for vibration reduction," *Journal of Sound and Vibration,* vol. 331, no. 14, pp. 3286-3303, 2012.

[49] R. Caliò *et al.*, "Piezoelectric energy harvesting solutions," *Sensors,* vol. 14, no. 3, pp. 4755-4790, 2014.

[50] S. Pobering and N. Schwesinger, "A novel hydropower harvesting device," in *2004 International Conference on MEMS, NANO and Smart Systems (ICMENS'04),* 2004: IEEE, pp. 480-485.

[51] E. Uddin and H. J. Sung, "Simulation of flow-flexible body interactions with large deformation," *International Journal for Numerical Methods in Fluids,* vol. 70, no. 9, pp. 1089-1102, 2012.

[52] W.-X. Huang, S. J. Shin, and H. J. Sung, "Simulation of flexible filaments in a uniform flow by the immersed boundary method," *Journal of Computational Physics*, vol. 226, no. 2, pp. 2206-2228, 2007.

[53] B. Audoly and Y. Pomeau, *Elasticity and Geometry*. Oxford University Press, 2010.